Increased backing softness of planar smooth dry adhesives enhances contact area and frictional load capacity on a cylindrical substrate

With bio-inspired backings: Solid, Sponge & Inflatable

Niels Glaser
Student number: 4376560

Mechanical Engineering, Bio-Mechanical Design, Bio-Inspired Technology
Delft University of Technology
Netherlands
22-07-2022

Supervisors:
Dimitra Dodou (Delft University of Technology, BMD)
Julian Langowski (Wageningen University & Research, Experimental Zoology Group)

A collaboration between the universities

Increased backing softness of planar smooth dry adhesives enhances contact area and frictional load capacity on a cylindrical substrate

Niels Glaser, 4376560

Abstract—Dry adhesives can reattach to surfaces due to the reversible bond made by Van der Waals forces. These adhesives can therefore be used as gripping surface that has a high frictional load capacity, independent of the grasping force. In many grippers, the adhesive surface is often pressed into contact with another surface ('substrate') in an open and closing motion. Since, generally, substrates have non-flat shapes, the adhesive has to be pressed into more directions at once to make full contact. An additional part to the adhesive system is needed here to transform the closing motion to a multi-directional preload on the adhesive surface. To realize this, a passive soft material behind the adhesive is added in this study.

Design objectives for such a material ('backing') were formulated and different types of bio-inspired backing concepts (solid, sponge, and inflatable) were fabricated. To gain insight in the suitability of these backing concepts with regard to some of the objectives, minimal required preload and minimal residual stresses to avoid detaching forces, two things are measured. Firstly, backing softness was measured as the compression stress-strain characteristic of the backing. Secondly, the preload contact stress distribution of backings was qualitatively measured.

The adhesive was a thin planar adhesive material reinforced with a planar mesh. One sponge backing type and one inflatable backing type were selected as practical backings to fabricate an adhesive system with. An experiment to measure frictional performance was done with these systems whereby backing softness was varied. These cuboid adhesive systems were pressed onto a cylindrical substrate and, after removal of the preload, loaded in the direction of the reinforcement while measuring frictional load capacity and contact area.

For both these two adhesive systems types, experiments showed that an increased backing softness caused an even or greater contact area throughout the whole loading cycle. The linear correlation coefficient, between rest phase contact area and maximum load capacity was 0.96, and at the end of the load phase, between the 'slide' contact area and 'slide' load capacity was 0.99.

With an inflatable or sponge backing design it is possible to make a softer backing compared to a solid design made by the same material. Only the sponge backing type distributed the preload relatively even at low and high compression, owing it to its stress plateau in its compression stress-strain characteristic. Although the inflatable has an equal pressure internally and also shows such a plateau, it was found that its contact stress is not even, due to the effect of its outer hull.

Concluding, the addition of a soft backing to help make and keep contact with a general shaped substrate, and thereby increasing load capacity, promises a new design paradigm in synthetic dry adhesives. Furthermore, the results indicates functional relevance of the presence of a relatively large and soft volume between the bones and the adhesive surface of the fingers/toe pads of geckos, tree frogs and humans.

Index Terms—Versatile attachment, Reinforced dry adhesive, Curved substrate, FTIR, Pressure distribution, Contact area, Bio-inspired, Fabrication, Silicone sponge, Inflatable

1 Introduction

Mankind tries to reproduce the sticking ability of animal such as tree frogs and gecko's since these adhesive bonds can be made and unmade multiple times [1, 2, 3, 4]. Research hints towards the importance of Van der Waals forces in the adhesive bonds of these animals (gecko [5], tree frog [6]). Van der Waals forces can cause attraction between atoms (or molecules) when the distance between these is small enough (nm scale). The synthetic adhesive systems inspired by these animals work therefore with Van der Waals forces. The tacky part of an adhesive system is called here the adhesive, and the surface it should stick to is called the substrate. The total adhesive force of the bond between adhesive and substrate increases when more atoms of the adhesive come into close range with the atoms of the substrate. For these systems to make contact with a substrate, it is therefore paramount that the adhesive can conform to undulations of the substrate on the micro-scale (roughness) as well as on the macro-scale (shape), and need therefore softness.

Softness usually refers to a surface property of a material. In this research, softness, and its reciprocate stiffness, refers to a bulk property of a material, giving a relation between deformations (strains) and stresses in the material.

Mechanical background synthetic dry adhesive systems

Whereas softness in compression is good, Bartlett et al. developed a general adhesive strength model in which softness of the adhesive in the load direction decreases the load capacity of the adhesive [7]. The load capacity is the force required to pull the adhesive system off the substrate. In short, the model assumes that elastic energy stored in the adhesive, due to the load, will balance the required surface energy when the bond brakes. Since more soft materials store more elastic energy at a given load ($\mathrm{Energy} = \mathrm{Load}^2 \cdot \mathrm{Compliance}$), the required surface energy for debonding is met at a lower load. Thus, allowing softness of the adhesive in certain directions to make contact with the substrate, while being stiff in the load direction, is key for making dry adhesives systems.

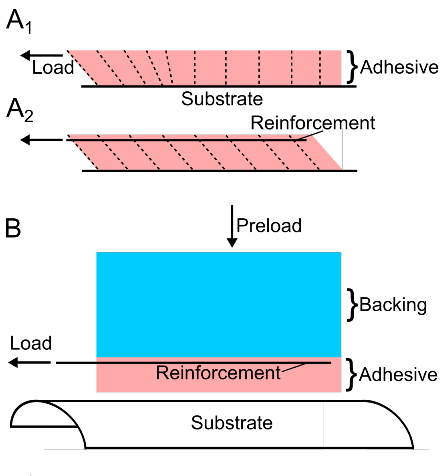

Fig. 1: A1: Schematic of an un-reinforced adhesive on a substrate under shear load. The dashed lines indicate strain (vertical lines indicate un-sheared material). Only the part in the adhesive close to the load application point is being loaded. A2: When a relatively stiff reinforcement is added, the whole adhesive material is strained equally and therefore equally loaded. B: Schematic of the adhesive system terminology and design used in this paper.

The adhesive should be loaded evenly to make optimal use of the bond strength. When an adhesive, consisting of a homogeneous material, is loaded, higher stress and strain occur near the load application point, see figure $1A_1$. This makes the bond fail by a propagating local failure (peeling) as described by Kendall's model [8]. To distribute load equally on the whole contact area, a relatively stiff material added to the adhesive is needed. This reinforcement has uneven internal stresses and strains like the homogeneous material described previously. These strains however, are small compared to the induced strains in the softer material part of the adhesive [9], see figure $1A_2$. Therefore, its load capacity, described by Crosby's model [10], scales linearly with contact area.

To conform to a rough substrate, a material with lower material stiffness can be used [11]. Another approach is bio-inspired surface micro-structures [12, 13] which reduce the effective (i.e., structural) stiffness of the material [14]. Furthermore, a low stiffness implicates low internal stresses that occur due to the (elastic) deformations the adhesive needs to make to conform to the shape of the substrate. These internal stresses due to elasticity try restore the adhesive to its original shape and therefore try to pull the adhesive from the differently shaped substrate.

The adhesive requirements of softness to conform to the substrate, and stiffness in the load direction, can conflict. When a rigid plate is used as reinforcement for the adhesive [4, 15, 16], the adhesive can conform to limited shapes and has a contact area scaling problem, since in theory, two rigid surfaces have only 3 contact points with each other. To solve the contradicting requirements, multiple smaller rigid plates can be used to increase conformability and scale the contact area up [4]. Also, continuous fibers can be used as reinforcement [7, 17], retaining the in-extensibility in their length but allowing for compliance in other directions. Another method is to use a reinforcement made out of stiffness-tunable materials (e.g. granular materials [18] or shape memory polymers [19]) which can conform to a substrate when they are soft and can be loaded when they are hardened.

When there are more load paths to the adhesive's tacky surface (e.g. multiple rigid plates or multiple fibers), uneven stresses between load paths are inevitable, for example due to surface irregularities or non-uniformity in the loading system [20]. Effort has been made to distribute load evenly between load paths with the help of pulleys [21, 22], whiffle trees [23], non-linear springs [4], and fluids [24, 16].

Research gap

Before being able to load the adhesive, the adhesive has to be pressed into contact. Since the reinforcement is preferably compliant in directions other than the load direction, the reinforcement can not be used to press the adhesive into contact. E.g. in the case of a fiber-reinforced adhesive, using the fibers to press is difficult since fibers buckle in compression.

Besides positioning in space, pressing an adhesive into full contact with a non-flat substrate requires multiple preload directions over the adhesive surface. This freedom is often not available and is e.g. restricted to an open-and-closing motion in manual grippers [25, 17] and soft pneumatic grippers [26, 27, 28]). Also, in robotics, movement actuators besides those for positioning in space, would add further complexity and weight. Thus an addition to the adhesive system is needed to help deform the adhesive to the substrate when there is only a preload available with one degree of freedom in movement. This addition will be called the 'backing' and together with the adhesive makes up the '(adhesive) system'. The backing is positioned behind the adhesive, if seen from the substrate, see figure 1B.

Previously, a soft sponge [16] and a spring on a gripping robot [15], were used as backing on top of a plate-reinforced adhesive. Since the plate was rigid these backings were used for alignment of the adhesive and were not deforming the adhesive. When the substrate has a different shape from the adhesive, both the adhesive and backing will have to be soft. Thus the status-quo in technology is that there is insufficient technology to conform to such substrates. A granular material reinforcement was simultaneously used as backing in its 'soft' state [18].

Aim of the study

This study aims to investigate the effect of varying the backing softness on the frictional performance of an adhesive system on a substrate that has a different shape, specifically making and keeping contact and the thereby resulting frictional load capacity. The adhesive is relatively thin compared to the backing which in turn has dimensions in the same order as the substrate's size. This implies that the adhesive can only make contact on the roughness level of the substrate, and contact made at the shape level is due to the backing component. The substrate in this study has a cylindrical shape to which a cuboid shaped adhesive system has to deform, see figure 1B. The adhesive system is initially pressed onto the substrate with a horizontal plate via the backing to make contact. This preload has one degree of freedom (up and down). After removing the preload the system is shear-loaded. The adhesive is flexible but inextensible due to its reinforcement. Furthermore, biological dry adhesive systems are reviewed for new bio-inspired backing concepts that will be used for the backing of the adhesive systems.

Hypotheses

As mentioned, a low stiffness implicates low internal elastic stresses that occur due to the deformations the system needs to make to conform to the substrate. These internal stresses tend to restore the adhesive to its original shape and therefore try to pull the adhesive from the substrate. Therefore, it is expected that the adhesive system with the softest backing layer performs the best since it experiences less internal stress at a given deformation, specifically:

1) A system with a softer backing makes more contact with a non-flat substrate at a given preload
2) A system with a softer backing keeps more contact with the substrate after removal of the preload, and thereby has a higher load capacity

Here it is assumed that a comparison is made between backings with a similar structure with similar internal stresses as well as relation between contact area and load capacity.

The study starts with the design of one type of adhesive and multiple types and variations of backings, their fabrication and then characterization (sec.2) with respect to design requirements and objectives. Afterwards, experiments are done to quantify the frictional performance (sec.3) for a selection of backings in combination with the adhesive. This is done for two parameters: (1) area of contact between the adhesive system and the substrate, and (2) frictional load capacity of the adhesive system. The adhesive is kept as a constant and backing softness is varied.

2 Design of adhesive systems

This section shows the design and fabrication of the adhesive, and multiple backing types and their variations. The key property of these backings, softness, is quantified as well as their distribution of contact stress with the substrate under a preload. The key property of the adhesive, load capacity, is also quantified. The section starts with requirements and objectives of the designs, which are summarized afterwards, continues with an existing concept for the adhesive and three bio-inspired design concepts for 7 backing types, shows the fabrication and characterization methods to quantify the properties, and ends with two resulting adhesive system types that are subsequently used in section 3.

From (sec.3.1.1) it follows that the adhesive design needs to fulfill 5 requirements to be suitable for the experiment. The first two requirements specify the topology and size of the adhesive. The third requirement is that the adhesive should at least stick to a cylindrical substrate. To increase its load capacity such that it does stick, two things can be done. Firstly, the tackiness of the adhesive can be increased by using a softer adhesive material [11]. Secondly, the bending stiffness can be reduced to mitigate internal stresses in the adhesive that try to peel the adhesive from the substrate. Bending stiffness can be reduced by using a thinner adhesive and reinforcement and using, again, a softer material for the adhesive material. Third requirement: dry adhesives have the benefit to reattach but this is also required to do multiple measurements with an adhesive system in the experiment. Repeatability of the adhesive can be increased by using a fine structured reinforcement which allows for a large and distributed bonding area with the adhesive material. The last requirement is that the adhesive surface is evenly loaded to make load capacity and contact area linearly related. Therefore a relatively stiff reinforcement should be used compared to the adhesive material softness, as explained in the introduction (fig.1)A2).

For the design of a backing there are two objectives (to strive for) and one requirement besides size. The two objectives are that the backing results in a minimal preload needed to conform the adhesive to the substrate, and subsequently after removal of the preload, that the backing does not pull the adhesive from the substrate. Material softness dictates to what extend a material will deform to undulations under a certain preload. After removing the preload, the deformed backing will have residual stresses that try to restore the backing to its original shape, and thereby try to peel the adhesive from the substrate. For both these objectives, a softer backing material will have a positive effect on the contact area made and contact kept with the substrate. The contact stress distribution under preload is another important parameter, since adhesives require a certain normal preload to make contact on the microscale (by pressing the surface roughness/structures onto each other). When the compressive preload is distributed over the whole contact area such that this compressive normal preload on the microscale is at this threshold, minimal total preload is required. Furthermore, when an adhesive system has made contact with the curved substrate and the preload is removed, the contact stresses between the adhesive and substrate will be compressive and tensile to balance each other. The measurement of this distribution is out of the scope of this study. The requirement of the backing is that it is suitable as variable for the experiment. This requires that the backing is able to be made in different softness variations, and the range of softness variations should be relatively big compared to its softness. Furthermore, the backing should in the end not be softer than the adhesive otherwise the adhesive will barely deform.

These requirements and objectives, with, if present, respective 'solutions/variables', are summarized as follows.

Adhesive requirements

- Sticks to a cylindrical substrate with a radius of $35\,\mathrm{mm}$ (sec.3.1.1)

1) High tackiness $\rightarrow$ Soft adhesive material
2) Low internal stress when conformed to substrate $\rightarrow$ Low bending stiffness $\rightarrow$ Soft and thin adhesive material, and thin reinforcement

- Reusable
  3) Should not fracture → Enough bonding area between adhesive material and reinforcement → Fine reinforcement structure
- Adhesive surface evenly loaded (sec.3.1.1)
  4) Reinforcement relatively stiff compared to adhesive material
- Topology; Planar adhesive with a planar reinforcement
- Size; Adhesive surface $50\,\mathrm{mm} \times 50\,\mathrm{mm}$

Backing design objectives

- Presses adhesive on substrate with a minimal preload
  1) Can conform to substrate shape → Soft backing
  2) No peaks in contact stress distribution during preload
- Does not pull adhesive from substrate after preload
  3) Low internal stress → Soft backing
  4) No peaks in contact stress distribution after preload (not in the scope of the study)

Backing requirements

- Backing softness as independent variable in experiment (sec.3)
  1) Can be made with different softnesses
  2) Range of different softnesses is relatively large compared to softness
- Size; Cuboid of $50\,\mathrm{mm} \times 50\,\mathrm{mm} \times 35\,\mathrm{mm}$

2.1 Conceptual design

In this subsection an existing adhesive design is adapted. Biological dry adhesive systems are reviewed for inspiration. With this inspiration, three backing design concepts are developed. The adhesive and backing bonded over their mating surface, will make an adhesive system as shown in figure 1B.

2.1.1 Adhesive

The adhesive used is a thin layer of a soft adhesive material reinforced with a mesh in the plane of the adhesive (schematic in fig.1B). The design is based on that of Bartlett et al.[7]. Due to the thinness of the mesh, the adhesive bends easily. The adhesive is loaded through this mesh. Since the mesh runs parallel to the adhesive surface, the adhesive is designed to resist shear loads. The free part of the reinforcing mesh is called the 'tail'.

2.1.2 Backing

Here, three biological systems that have adhesive grasping surfaces, tree frogs, gecko's and humans, will be looked at for similarities in the structure of their 'backing' regions. The underlying material in these systems is complex in structure and material properties, and are here modelled in different ways, which are: a solid, an inflatable (i.e. fluid contained by a hull), and an open celled sponge.

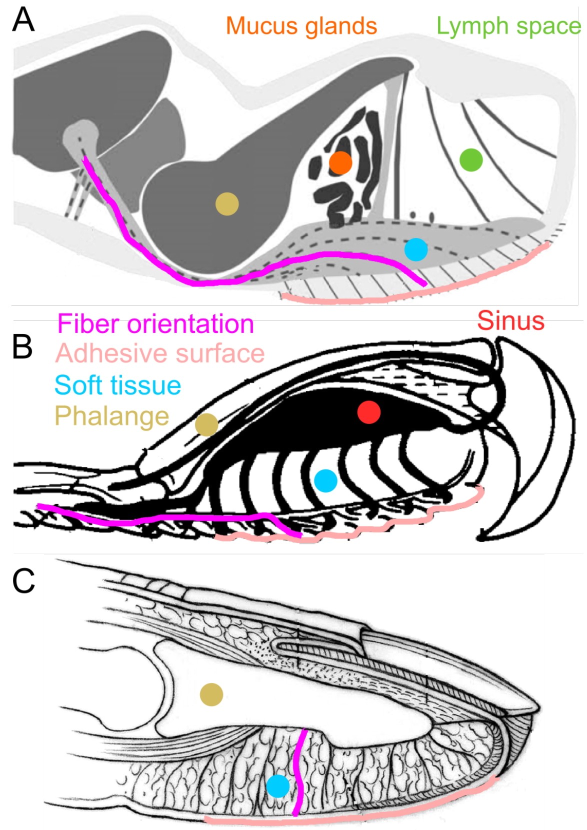

Fig. 2: Schematic representation of the digital pad/fingertip in the midsagittal plane of a tree frog (A), gecko (B), and human (C). A, B and C adapted from [29], [30] and [31] respectively.

Biological dry adhesive systems

The three examined biological systems can extend or flex their most distal finger/toe phalanx by means of connected tendons (gecko [32], frog [33]). This results in an open and closing motion that can be realised, as is the case in many synthetic grippers. Thus also these biological systems have to distribute the one-dimensional preload of the phalanx to a multi-dimensional preload on their adhesive surface to conform it to a substrate. The bio-systems are divided in a presumed adhesive part (adhesive material and reinforcement) and backing part, and their constituents presented.

The adhesive part of the frog is summarized as the following. The adhesive surface of a tree frog's pad bears surface micro-structures (hierarchical pattern of hexagonal beams) which are relatively short and thick [34]. These beams can bend individually to presumably form close contact with the inherently rough substrate [6]. Furthermore the tree frog's amphibian skin materials are relatively soft (pad stiffness $\approx 40\,\mathrm{kPa}$ [6]). Stiffer fibers reinforce these soft structures and connect, via an intermediate interface, to a tendon complex, which runs parallel to the adhesive surface [29]. These tendons connect to the second most distal phalanx [29]. Between this adhesive part and the most distal phalanx, sits connective tissues, mucus glands and a (fluid filled) lymph space [35]. See figure 2A for a schematic of the frog's adhesive system.

TABLE 1: Results, and experimental conditions

Backing characterization (section 2)

Backing type	Variations	Compression Modulus[a] [kPa]	Preload contact stress characteristic between backing and substrate	Used in experiment (section 3)
Hydrogel	H-4 H-3 H-2	$6.5_{40\%}$-$15.8_{40\%}$		No, impractical
Silicone	S-4/20 S-20/20 S-20/16 S-20/14 S-20/12 S-20/10	$10.0_{40\%}$-$104.5_{7\%}$	S-20/14; Shows relatively even (at low compression strain) or uneven (at high compression strain) stress distribution	No, stiff
Inflatable	I-O1 I-O2 I-O3 I-C1 I-C2 I-C3	$1.2_{40\%}$-$12.4_{17\%}$	I-O2 and I-C2; Shows peak stresses	Yes, soft, and enough range in softness
PUR-sponge	P-H P-M P-S	$3.5 \pm 0.1_{40\%\mathrm{f}}$-$5.6 \pm 0.0_{40\%\mathrm{f}}$	P-S; Shows relatively even stress distribution	Yes, soft, and enough range in softness
Sponge by mixing	M-20/16 M-20/15 M-20/14 M-20/13	$4.0_{40\%}$-$8.9_{40\%}$	M-20/16; Indicates fabrication artifact	No, stiffer than sponge by vacuum infusion
Sponge by vacuum infusion	V-20/20 V-20/16 V-20/15 V-20/14 V-20/13	$1.3_{40\%}$-$8.4_{40\%}$	V-20/20; Indicates fabrication artifact	No, geometric unstable
Sponge by foaming	F-1/5 F-1/3.5 F-1/2-1 F-1/2-2 F-1/2-3	$1.2_{40\%}$-$19.4_{40\%}$		No, inconsistent structure
Rigid	R-F R-C		R-F and R-C Show peak stresses	Yes, as control group

[a] Extremes of all variations

Experiment (section 3), and adhesive characterization (section 2)

	Variations	Specimens	Repetitions	Preload[b] [N]	Load capacity [c]	r [e]	Result
Adhesive		26	3	Manual to full contact	$M_{\mathrm{Av}} = 53.3(5.5)\mathrm{N}$ $M_{\mathrm{Av}} = 2.1\,\mathrm{N/cm^2}A_{\mathrm{r}}$[d] $S_{\mathrm{Av}} = 33.4(1.1)\mathrm{N}$ $S_{\mathrm{Av}} = 1.3\,\mathrm{N/cm^2}A_{\mathrm{s}}$[d]	0.21 0.07	Variable load capacity; use 5 specimens per system variation
Adhesive		1	30	Manual to full contact	$M_{\mathrm{Ar}} = 47.1(1.3)\mathrm{N}$ $S_{\mathrm{Ar}} = 33.5(1.6)\mathrm{N}$	0.06 0.10	Adhesive suitable for repeated use
PUR-sponge$_{\mathrm{S}}$	P$_{\mathrm{S}}$-H P$_{\mathrm{S}}$-M P$_{\mathrm{S}}$-S	5 per variation	3 per specimen	3.61, 0.01	$M_{\mathrm{P}} = 0.3\,\mathrm{N} + 2.2\,\mathrm{N/cm^2}A_{\mathrm{r}}$ $S_{\mathrm{P}} = -1.9\,\mathrm{N}+1.5\,\mathrm{N/cm^2}A_{\mathrm{s}}$	0.96[f] 0.99 [f]	A softer variation makes the same or more contact
Rigid$_{\mathrm{S}}$	R$_{\mathrm{S}}$-F R$_{\mathrm{S}}$-C	5 per variation	3 per specimen	3.61, 0.01	$M_{\mathrm{R}} = 2.0\,\mathrm{N} + 1.8\,\mathrm{N/cm^2}A_{\mathrm{r}}$ $S_{\mathrm{R}} = 0.2\,\mathrm{N} + 1.2\,\mathrm{N/cm^2}A_{\mathrm{s}}$	0.96[f] 0.99 [f]	Makes less contact than PUR-sponge$_{\mathrm{S}}$
Inflatable$_{\mathrm{S}}$	I$_{\mathrm{S}}$-C1 I$_{\mathrm{S}}$-O1 I$_{\mathrm{S}}$-C2 I$_{\mathrm{S}}$-O2 I$_{\mathrm{S}}$-C3 I$_{\mathrm{S}}$-O3	All variations use the same specimen	5 per variation	1.66, 0.01	$M_{\mathrm{I}} = 2.3\,\mathrm{N} + 1.6\,\mathrm{N/cm^2}A_{\mathrm{r}}$ $S_{\mathrm{I}} = -0.1\,\mathrm{N} + 1.3\,\mathrm{N/cm^2}A_{\mathrm{s}}$	0.96 0.99	Open variation makes more contact than the respectively closed variation. With lower internal pressure (softer backing) the same or more contact is made

[b] (Mean, 3 standard deviations relative to the mean)
[c] The M in e.g. M_{P} stand for maximum load, the S in e.g. S_{P} stand for slide load, A_{r} is the rest contact area, A_{s} is the slide contact area.
[d] Calculated at an estimated contact area of $25\,\mathrm{cm}^2$.
[e] Error of the load capacity with two meanings: 1) Relative error of two standard deviations from the mean to the mean. 2) Correlation coefficient between contact area and load capacity (rest phase, load phase)
[f] Data of PUR-sponge$_{\mathrm{S}}$ and Rigid$_{\mathrm{S}}$ is taken together to calculate correlation coefficients.

The adhesive part of the gecko is summarized as the following. The gecko's adhesive surface is made from b-keratin which is stiff (tensile elastic modulus of 1-3 GPa [36]). This surface can still conform to a substrate due to the presence of surface micro-structures (branching beams) which are relatively slender [37]. These structures connect, via an intermediate tight interface, to the lateral digital tendon complex, which runs parallel to the adhesive surface [32]. The tendon complex connects directly to the skeleton (not the most distal phalanx) by joint capsules [32]. Between this adhesive part and the most distal phalanx, sits connective tissues, spring-like [38] soft lamellar skin [5], and a large sinus [30]. This sinus is filled with blood and connects to the vascular system [5]. See figure 2B for a schematic of the gecko's adhesive system.

The adhesive part of a human can be summarized as follows: Friction of human skin against glass is known to be principally due to adhesion [39, 40]. Human skin has a softness of $\approx 100\,\mathrm{kPa}$ (stratum corneam [41]) and becomes softer by sweating ($\approx 25\,\mathrm{kPa}$, wetted stratum corneam [41]). Since the presence of fluid between the skin and substrate can cause a reduction in friction [39, 40], the fingerprint structure may aid in removing fluids between the skin and substrate. Fibers run in the (epi)dermis mainly parallel to the adhesive surface [42]. Fibers also extend from the most distal phalanx radially to the dermis [31]. Between the adhesive ((epi)dermis) and phalanx sits, besides the latter fibers, also pulp (fat) that constitutes over half the fingertip volume [31]. To this pulp run arteries that branched off at the most distal interphalangeal joint [31]. See figure 2C for a schematic of the human's adhesive system.

The presence of a relatively large and soft volume between the pre-load point (phalanx) and adhesive surface of the presented bio-systems, suggests functional relevance of such a soft volume for dry adhesive systems.

Bio-inspired backing design concepts

Three soft backing design concepts are derived here.

2.1.2.1 Solid:

To imitate, in a simplified form, the soft bulk material found in the the biological systems, e.g. the pulp and other connective tissues, the concept of a solid backing design is formed.

It is expected that the solid will show a strictly increasing relation between compressive strain and internal stress, and therefore that the contact stress distribution is uneven.

2.1.2.2 Inflatable:

For the frog it may be possible that the fluid in the lymph space is able to escape to other parts of the lymphatic system, like the blood in the sinus of the gecko can to its vascular system, or like the blood in the fingertip of a human. When such a fluid can escape the fingertip / toe pad, the fluid pressure would not increase and the enclosing dermis is able to deform more freely. An illustration of this would be when pushing a human fingertip onto a substrate; blood is pushed out of the tip, turning the finger white, and will flow back after detachment. This is suspected to make the backing soft and thus implies better conformability to a substrate. When the case is taken that the fluid regions are part of a circulatory system, the fluid would be free to leave the adhesive system at a certain overpressure threshold. When the opposite case is taken, the fluid is not free to leave the adhesive system. The inflatable concept will therefore consist of a fluid enclosed by a compliant hull, in which the fluid can either not leave the hull, or leave and enter the hull at a controlled pressure threshold.

A stationary fluid has the property that pressure is even in its volume, and has no softness since it cannot hold shearing forces. It is suspected that these properties help to distribute the preload evenly while adding negligible stiffness to the backing. A fluid, however, has to be contained by a hull, and this hull will negatively affect the contact stress distribution and softness.

In the case of the tree frog and gecko the fluid is a liquid, which is usually taken as an incompressible material. Overpressures relative to ambient pressure in the inflatable were expected to be less than a couple percent. At those overpressures air may be considered incompressible. Air is preferred due to its lower weight.

2.1.2.3 Sponge (open celled):

The last concept is that of an open celled sponge, which is assumed to imitate in a simplified form the spring-like soft lamellar skin of the gecko, and the fluid rich biological backings when these are seen as a set of smaller fluid regions separated by 'spongeous' connective tissue. Simplified, the connective tissue might behave as a open celled sponge, in which a fluid is able to freely pass through the sponge. The unsupported cell walls (the tissue) buckle easily and the sponge can therefore elastically deform to large strains in compression. In tension, however, the walls will not buckle and the sponge can therefore be relatively stiff if its material is.

Synthetic fingertips, with a sponge material to simulate the pulp, have been used to imitate human fingertips. These showed similar mechanical behavior [43].

Due to the buckling of the cell walls likely happening for a large strain interval, which means that internal stress slightly increases, it is expected that the contact stress distribution at this interval is relatively even.

2.2 Fabrication of adhesive and backings

This subsection describes the fabrication of 7 different backing types based on the 3 design concepts. Also, a rigid backing design concept is fabricated for comparison purposes. The resulting rigid backing type has two variations in shape instead of softness, a curved one and flat one. For the solid concept there are two types made, a solid gelatin hydrogel, since hydrogels are often seen in nature, and a more practical solid, silicone, that might have similar softness behavior. Variations in softness for these are made by varying the gelatin content or silicone mixing ratio. For the inflatable concept, one inflatable type is made, which has three softness variations for the 'open Inflatable' in which air can leave and enter the hull (constant internal pressure), and three softness variations for the 'closed Inflatable' in which air cannot leave the hull. Softness in the open and close Inflatable is varied by changing the initial inner pressure. For the sponge concept, there are four types. One type is a commercially available PUR-sponge, and the other three types are made with silicone with different fabrication methods to get different sponge structures. These fabrication methods are 'mixing with a soluble', 'vacuum infusion into a soluble', and 'foaming'. Variations in softness for the types made by mixing and vacuum infusion are made by changing the silicone mixing ratio while for the foaming type it is by process parameters. The commercially available PUR-sponge comes in different softness grades.

2.2.1 Adhesive

The adhesive is based on the design of Bartlett et al. and consists of silicone (Silicone rubber shore hardness A8 (Resion siliconen gietrubber addition cure, 8A)) reinforced by a polyester mesh (100 g/m^{-2}, midge mesh, 18x30 holes per square inch). To make the adhesive more tacky, the silicone was made by mixing 4 parts 'a' with 20 parts 'b', instead of the normal 20/20 ratio. Furthermore, white pigment was added to make the silicone more opaque for imaging purposes in the experiment (1 wt% silicone pigment white from www.Siliconesandmore.nl). It was manufactured by stacking the mesh between two $0.5\,\mathrm{mm}$ thick polystyrene cut-outs on top of a glass panel, see figure 3A. Between the glass, mesh, and polystyrene, a seal of petroleum jelly (Vaseline) is smeared. In each cut-out is then silicone poured until the cavity is filled till the top edge, see figure 3B&C. The cut-outs have a surface area of $5\,\mathrm{cm} \times 5\,\mathrm{cm}$. After pouring, air bubbles rise to the top due to their buoyancy and some stuck below the reinforcement are manually poked with a pin to help with rising. The adhesive became approximately $2\,\mathrm{mm}$ thick. After curing, the mesh with silicone is pulled from the glass and cut into strips, giving the adhesive a 'tail' with a length of 20 cm, see figure 3D. These were then washed with alcohol and rinsed with water, to remove the jelly from the

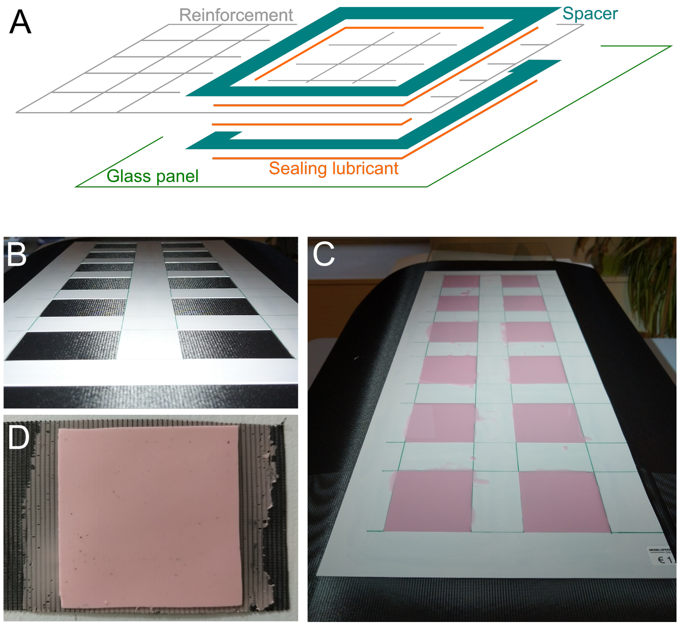

Fig. 3: Fabrication of the adhesive. A: Schematic of the mould for a single specimen. B: Top-view of the finished mould. The friction between the reinforcement and the petroleum jelly prevents the reinforcement from sagging. C: Silicone is poured into the holes of the spacers. D: Finished adhesive after being cut to size.

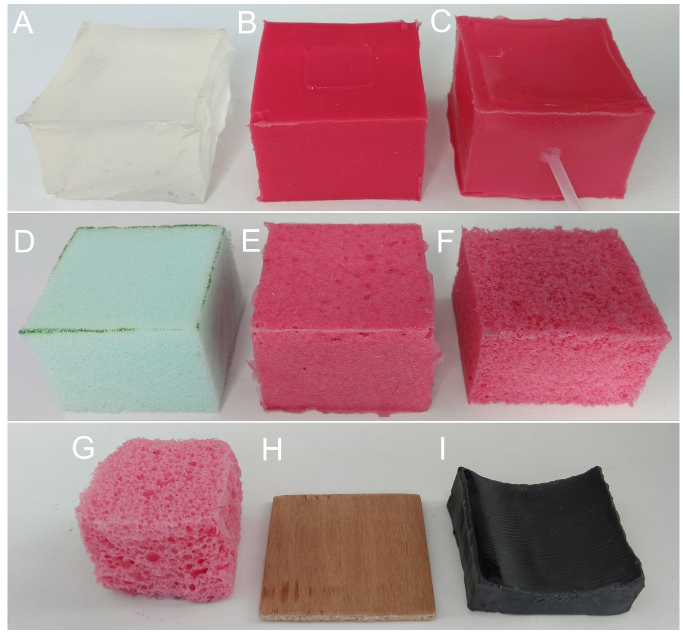

Fig. 4: Investigated backing types. A: Hydrogel, shown variation is H-3. B: Silicone, variation S-20/14. C: Inflatable. Via the tube the inside of the hollow silicone cube can be pressurized. D: PUR-sponge, variation P-S. E: Sponge by 'mixing, variation M-20/16. F: Sponge by vacuum infusion, variation V-20/20. G: Sponge by foaming, variation F-1/2-3. H: Rigid backing type, flat variation (R-F). I: Rigid backing type, curved variation (R-C).

tail. The flat silicone surface that cured onto the glass was used as the adhesive surface.

2.2.2 Backing: solid concept

Two types of the solid are made. A gelatin hydrogel since water and collagen are often found as building blocks in biological tissue, and a silicone solid since this is likely a more practical material which might show the same softness characteristics as the hydrogel.

2.2.2.1 Hydrogel:

Gelatin cubes ($5\,\mathrm{cm} \times 5\,\mathrm{cm} \times 3.5\,\mathrm{cm}$) were made by pouring gelatin (hydrolyzed collagen) into an open paper box with the same dimensions. A plastic foil was placed into the box to make removal from the box and displacing the gelatin easier. The gelatin was prepared by adding gelatin sheets (Dr. Oetker Gelatine) to warm water and stirring till they dissolved. After cooling down for $3\,\mathrm{h}$ in a fridge, the solution became solid. Different weight ratios of gelatin to water were used (2 wt%, 3 wt%, and 4 wt%) to vary hydrogel softness. The gelatin materials are called 'H-x', where 'H' stands for 'Hydrogel' and 'x' for the gelatin-weight percentage. See variation H-3 in figure 4A.

2.2.2.2 Silicone:

Silicone cubes were made by pouring silicone (Resion siliconen gietrubber addition cure, 8A) into an open paper box. It cured at room temperature for at least 24 h. Different parts 'a' to parts 'b' ratios of the two part silicone were made to vary silicone softness. The silicone materials are called S-a/b, were 'S' stands for 'Silicone', 'a' for parts a, and 'b' for parts b. See variation S-20/14 in figure 4B (others variations are shown in apx.A fig.20A). At a mixing ratio of 20/10 the silicone is nearly solid and becomes very brittle when being handled. The more the mixing ratio differs from the normal 20/20 ratio (either more part a or part b), the tackier they feel with touch.

2.2.3 Backing: inflatable concept

To make a cube shaped hull with dimensions of $5\,\mathrm{cm} \times 5\,\mathrm{cm} \times 3.5\,\mathrm{cm}$ and a wall thickness of $1\,\mathrm{mm}$, a multi-part mould was made, see figure 5A&B. The mould parts were sealed with putty (plasticine, Siliconeandmore.com), the mould was placed on an incline, and silicone was poured into the lower opening, forcing the air to leave via the higher opening, see figure 5C. Since the inner cube part of the mould is connected to the outer parts of the mould, this connection gives a hole in the cured hull through which the inner cube can be taken out. This hole is closed by gluing a $1\,\mathrm{mm}$ thick silicone slab onto this side with uncured silicone. Vacuuming the just mixed uncured silicone was done to reduce the occurrence of gas bubbles in the hull. A silicone tube (inner diameter $2\,\mathrm{mm}$, outer diameter $3\,\mathrm{mm}$) was glued (Elastosil, E43 Wacker silicones) into an incision in a wall of the hull. The resulting Inflatable weighs 14 g and is shown in figure 4C.

To make the open inflatable variations, a relatively large air reservoir is connected to the inflatable into which the air can escape (fig.6). Air (and pressure) is added with a pump, and a valve (clamp on the tube) can close the reservoir off. To make the closed Inflatable variations, the valve next to

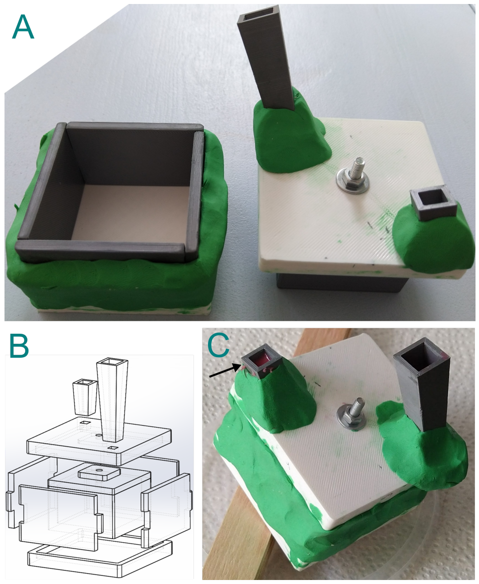

Fig. 5: Mould used to fabricate the Inflatable. A: 3-part mould consisting of an inner cube connected to the top part with a spacer, and a bottom part. The bottom part consist of multiple pieces (B) to help with removing the cast. The green putty seals the connections. C: The mould is placed on an incline such that the air outlet (arrow) is the highest point. Silicone is poured into the longer inlet.

the Inflatable is closed. The open Inflatable is called 'I-Ox', and the closed inflatable is called 'I-Cx', were 'x' refers to the over-pressure in 100 Pa or equivalently cm height of the water column of the pressure sensor. Three initial over pressures are used for both the closed and open variations, namely 100, 200 and 300 Pa.

To regulate the pressure inside the Inflatable, a water column pressure sensor is added between the air reservoir and the Inflatable. The tube is connected to the outlet of the outer part of a syringe, which sits in the water, see figure 6. Drawn on this outer syringe part, are distances from the water surface. When pressure in the inflatable increases, the water is pushed out the syringe. Since the water surface is much greater than the cross section of the syringe, the increase of water level (the zero level) is negligible.

The open variations use the reservoir which has a finite volume (garbage bag, Komo Huisvuilzakken 50 L) and, therefore, the pressure in the reservoir (and in the Inflatable) will increase when the Inflatable is compressed. Due to the relatively large volume of the reservoir compared to the Inflatable, the total volume of the reservoir with open Inflatable is relatively unaffected when the Inflatable is fully compressed. With an estimated reservoir volume of 45 L, the increase in pressure when the Inflatable is fully compressed, is approximately $0.15\,\mathrm{kPa}$, equivalent to an increase of $1.5\,\mathrm{cm}$ water head $(\text{pressure} = \text{gravity} \cdot \text{density} \cdot \text{height})$.

$(V_I + V_R) \cdot P_s = P_e(V_R) = (P_s + P_i)V_R$, where V_I, V_R, P_s, P_e, P_i are the Inflatable volume, reservoir volume, starting pressure, ending pressure, and increase in pressure respectively,
$P_i = P_s \cdot V_I/V_R = 100.3\,\mathrm{kPa} \cdot (0.48 \cdot 0.48 \cdot 0.33)/45 = 0.15\,\mathrm{kPa}$,

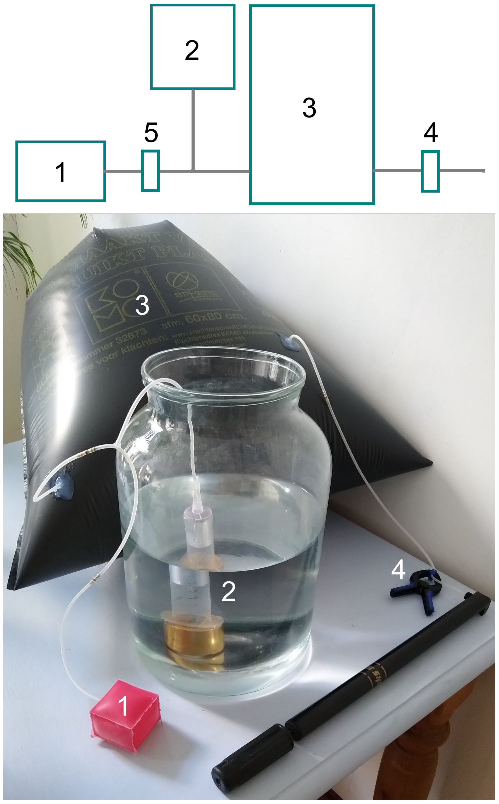

Fig. 6: Setup used to make softness variations of the Inflatable. The Inflatable (1) is connected to a water column pressure sensor (2) and air reservoir (3) via tubes. The reservoir is also connected to the air inlet which can be closed off with a clamp (4). A hand pump is connected to the air inlet. To set up the open Inflatable variations, air is pumped into the inlet until the pressure sensor reads the variation's specified initial pressure, and then the clamp (4) closes off the tube. The same is done to set up the closed Inflatable variations but here a clamp (5, shown in the schematic) is placed on the tube a couple centimetres from the Inflatable.

For all used initial overpressures (0.1, 0.2, 0.3 kPa) this is approximately the case.

Since this effect is present for all open variations, these variations can still be compared with each other. In the the supplement movie 1, the open Inflatable I-O2 is shown during full compression and relaxation. The video shows an increase of just $0.5\,\mathrm{cm}$ water head instead of the estimated $1.5\,\mathrm{cm}$.

2.2.4 Backing: sponge concept

For the sponge concept there are 4 types made. Commercially available PUR-sponges are chosen since these are soft up to high strains. Since polyurethane (PUR) is not such a soft material for the sponge, it is expected that PUR-sponges can be relatively stiff in tension. Therefore, also sponges are made with silicone, which is softer and has a higher elastic strain (>100%) than PUR. A silicone sponge will be fabricated in three different ways which each gives a backing type. This is done since these fabrication methods were not explored for the silicone used and methods affects the sponge structure and in turn its softness.

2.2.4.1 PUR-sponge type:

PUR-sponges were cut from larger sheets with a knife. The sponges are called 'P-x', where 'x' refers to its softness rating and 'P' to 'PUR-sponge'. The ratings are 'S' (Soft)(traagschuim SG 65, Schuimrubbergigant.nl), 'M' (medium)(Nasa foam - traagschuim SG 57, Schuimrubberbetaalbaar.nl), and 'H' (Hard)(traagschuim SG 50 grey, Schuimwinkel.nl). See figure 4D for variation P-S.

2.2.4.2 'Sponge by mixing':

An open celled sponge can be made by mixing an uncured material, in liquid form, with soluble solid grains. After curing, the workpiece is placed in a solvent to dissolve the solid. Here, silicone, sugar (Kristalsuiker, Van Gilse), and water were used. An estimate for the packing fraction of the sugar grains is 0.6 ($50\,\mathrm{ml}$ in measuring cup has a mass of $47.54\,\mathrm{g}$, which gives a density of $0.95\,\mathrm{g\,cm^{-3}}$, the density of sugar is $1.59\,\mathrm{g\,cm^{-3}}$. Due to the grains touching each other when tightly packed, the solvent can reach all grains after the silicone has cured, which makes it open celled. No hard parts (where crystal sugar exists) were noticed by touch. To vary sponge softness, the silicone was mixed in different ratios, while keeping the sugar packing fraction constant. Variation M-20/16 is shown in figure 4D (other variations are shown in apx.A fig.20B). The sponges are called 'M-a/b', where 'a' refers to the silicone parts a and 'b' to parts b. The sugar grains were mixed with 0.4 total volume fraction silicone, and put into an open paper box of the envisioned sponge dimensions. When a smaller (0.15) total volume fraction of silicone was used (to make an even softer sponge), a hollow sponge formed (see apx.A fig.20C).

2.2.4.3 'Sponge by vacuum infusion':

It is also possible to use a sugar cube instead of loose grains and infuse it with uncured liquid silicone [44]. After curing the sugar cube is dissolved. This way the sugar packing ratio is expected to be higher than with mixing. Due to the small channels the silicone has to travel through, the silicone needs a driving force when the sugar cube is larger than a normal thea sized cube. A refrigerator compressor was used to make a vacuum on one side of the cube. Four other sides were closed off with duct-tape and the duct-tape made a container on the remaining side of the cube, in which silicone is poured, see figure 7. The sugar cubes were made by adding one gram water per 18.9 gram of sugar grains (Kristalsuiker, Van Gilse), stirring the mix, scooped into a paper box with the envisioned sponge dimensions, and left to dry. Different mixing ratios of the silicone were used to vary sponge softness. Sponges made with small cubes ($33\,\mathrm{mm} \times 33\,\mathrm{mm} \times 30\,\mathrm{mm}$) are called 'V-a/b', where 'a' refers to the silicone parts a and 'b' to parts b (see apx.A fig.20D). There were also sponges made with bigger sugar cubes ($50\,\mathrm{mm} \times 150\,\mathrm{mm} \times 35\,\mathrm{mm}$), these would take weeks to dry by air and were therefore placed 4 times in a microwave at 500 W for 1:40 min. Too long or at a higher wattage in the microwave melted the sugar. Three variations were made with a bigger cube, with mixing ratio 13/20 (called V_x-13/20), with mixing ratio 14/20 (called

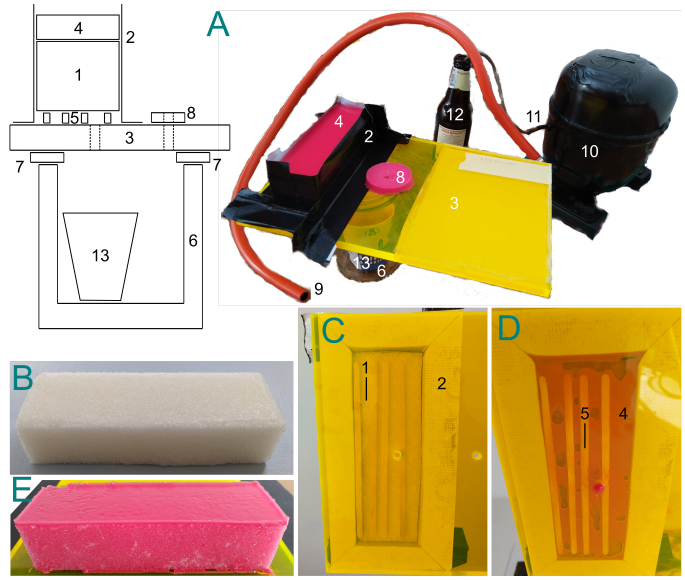

Fig. 7: Vacuum infusion process for the fabrication of open celled silicone sponges. A: Vacuum infusion setup used to create silicone sponges. Shown on the left is a schematic of part of the setup, and shown on the right is a photo of the setup. A sugar cube (1) is taped (2) with its sides to a panel (3). The tape creates a reservoir on top of the sugar cube which is filled with uncured silicone (4). In between the sugar cube and panel are spacers (5) to allow air and silicone to flow into a hole in the panel that ends up in a glass pot (6). In between the pot and the panel sits a silicone ring (7) to make an airtight connection. Another hole in the panel connects the air inside the pot with another silicone ring (8). The ring (8) connects to the air inlet (9) of the vacuum pump (10). The pump's air outlet (11) is stuck into a bottle (12) to catch oil droplets. When the pump runs, air is sucked from the underside of the sugar cube, and the silicone is pushed into the cube by the atmosphere. When the cube is being infused with silicone, silicone may drip through the hole but falls into a cup (13) while air can move into the air inlet. B: Sugar cube of size $5\,\mathrm{cm} \times 15\,\mathrm{cm} \times 3.5\,\mathrm{cm}$. C: Sides of the sugar cube taped to the panel to create an airtight connection. The wooden sticks act as spacers to allow the flow of silicone and air to the hole. D: Sugar cube after vacuum infusion with silicon. E: Sugar cube after vacuum infusion with silicon.

V_x-14/20), and with mixing ratio 20/20 (called V-20/20, in the same manner as the small ones)(see apx.A fig.20E). V_x-13/20 and V_x-14/20 did not keep the dimensions of the sugar cube when the sugar was dissolved. V-20/20 seemed to have a different structure in its center (see apx.A fig.20F). The volume fraction of the sugar in the sugar cubes is 0.69. (Sugar has a density of 1.59 g/cm3. The small sugar cubes had a weight of 40.3, 40.32 & 41.3 g which gives a density of 1.12-1.15 g/cm3 and a volume fraction of 0.68-0.7. The bigger sugar cubes had a weight of 284, 291, 288 & 292 g which gives a density ratio of 0.69-0.7.) Variation V-20/20 is shown in figure 4E.

2.2.4.4 'Sponge by foaming':

A silicone sponge can also be created when the silicone is cured while there is a foaming agent creating gas bubbles inside the uncured liquid silicone. This method was used with the expectation that the total cell volume would be higher than with the dissolving crystal methods, and thereby creating softer sponges. The foaming recipe (based on [45]) consisted of baking powder (bakpoeder Dr. Oetker Backin), citric acid (half the weight of baking powder; Citroensap Polenghi), and a couple of droplets of dish detergent (Eco afwasmiddel, Klok). The foaming ingredients were added to the silicone parts in an open paper box, which was placed in a household oven or microwave for faster curing. The specimens are called F-r(-n), where 'r' refers to the weight of the baking powder compared to the weight of the silicone, and 'n' to the specimen number if applicable. Specimen F-1/2-2 is shown figure 4G (other specimens are shown in apx.A fig.20G). Due to the experimental nature of these attempts, process parameters (oven temperature, location in/on the oven, microwave power and time, heating the silicone before adding foaming agents, amount of dish detergent) varied for each specimen. It proved difficult to make consistent specimens. Usable parts of the specimens were cut out (apx.A fig.20H).

2.2.5 *Backing: rigid design*

Lastly, also a rigid backing type was made for comparison purposes and control group. There are two variations, a flat and curved one.

A flat backing was made by cutting $3\,\mathrm{mm}$ thick plywood to $50\,\mathrm{mm} \times 50\,\mathrm{mm}$, weighing 7 g, see figure 4H. This materials is called R-F (rigid-flat).

A rigid backing with a curved side, see figure 4I, was made by pouring polyester onto a curved surface. The liquid polyester was contained by a wall of putty. This material is called R-C (rigid-curved). The polyester (polyester giethars, Resion) was used with 2 wt% hardener and 2 wt% black pigment (Resion polyester pigmentpasta black). The samples weigh approximately 30 g. The curved surface onto which the polyester is poured, is the top side of an adhesive which adheres to the curved substrate, see figure 8.

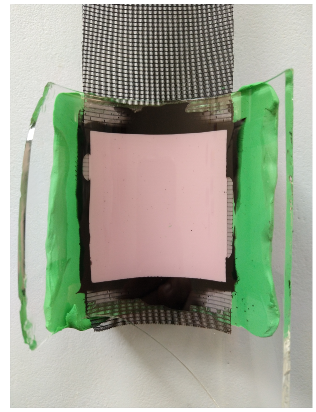

Fig. 8: Fabrication of the backing 'R-C' that has a concave side. Shown in the photo is the underside of the mould after the polyester cured. Green is putty, black is polyester or the adhesive tail, and pink is the adhesive material

2.3 Methods for material characterization

To check whether the fabricated adhesive fulfills the design requirements, its frictional load capacity on the curved substrate is measured. To characterize 'softness' of a backing, its stress as function of compression strain is measured. From the resulting stress-strain characteristic, compression moduli are calculated which will be used as general proxy for its softness. The contact stress distribution characteristic of the backings, under a preload, has preferably an even distribution as noted in the design objectives. This distribution is measured with a pressure sensitive film in between the backing and substrate.

2.3.1 *Adhesive: frictional load capacity*

To characterize the adhesive, its load capacity is measured in two ways. Firstly, to check how strong the adhesive is and how variable this is between specimens. Secondly, to check whether the adhesive keeps this performance with multiple uses. For the first way, the load capacity and its variability between manufactured specimens is measured, this is called the 'variability measurement'. Twenty-six specimens were each measured for 3 consecutive repetitions. With all combined repetitions the results are calculated. For the second way, the load capacity and its variability of one specimen is measured, this is called the 'repetition measurement'. This is done by measuring for 30 consecutive repetitions with one specimen.

Since the adhesive is designed to resist forces in the direction of its reinforcement, the load will be in this same direction. This is the direction of the adhesive's tail. The substrate used is a glass cylinder which long axis runs parallel to the tail of the adhesive. The adhesive is pressed manually into full contact with the substrate via an unconnected cuboid sponge (P-H) with a flat sliding platform, see figure 15C. To measure the load, the tail is clamped via a force sensor to a linear actuator that displaces $9\,\mathrm{mm}$ in the direction of the cylinder's long axis (for more detail see section 3.1.4).

It is expected that an adhesive is stuck on the substrate until the load reaches a maximum at which the adhesive starts sliding over the substrate under a lower load. This maximum load will be called the maximum load. The load at the end of the load measurement is called the slide load.

2.3.2 *Backing: compression stress-strain characteristic*

To characterize 'softness' of a backing, its stress as function of compression strain is measured. From the resulting stress-strain characteristic, compression moduli can be calculated which will be used as general proxy for its material softness. The compression modulus is stress over strain. When the characteristic is non-linear, the modulus varies with strain. Therefore, the modulus will be calculated at two strain values. These values are somewhat arbitrarily chosen. The higher value is chosen as 40% since most backings could be measured to this value (higher strains were limited by actuator travel, fracture, or force sensor limit). The lower value is chosen as 17% strain since this corresponds to a compression strain used in the 'preload contact stress characterization' measurement. One specimen per backing variation is measured. Although measuring one specimen per backing variation to quantify its softness gives no expected value, the goal here was to get a sense of the range of softness possible for a backing type. The trend of softness per backing variation, when one parameter is changed e.g. silicone mix ratio or gelatin content, becomes more clear with more backing variations. Since the softness of the PUR-sponge type is not varied in this study but different commercial PUR-sponges are bought for this purpose, 3 specimens per PUR-sponge variation are measured. All Inflatable variations use the same specimen and therefore do not require multiple measurements per variation to quantify their softness.

The fabricated backing variations are compressed between two flat plates. One plate is stationary and the other is attached to a linear actuator with a force sensor in between (for equipment details see sec.3.1.4, for the setup see apx.A fig.21). The velocity of the plate is $0.5\,\mathrm{mm\,s^{-1}}$ and its acceleration is $0.2\,\mathrm{mm\,s^{-2}}$. The plate stops at a set distance depending on specimen height. The return stroke starts after 1-2 s with the same settings. The PUR-sponges are also measured on their return stroke since these are known to have visco-elastic behavior which changes their stiffness after compression [46]. Stress is calculated by dividing the measured force by the original cross-section of the specimen. Strain is calculated by dividing the distance travelled by the plate, by the original height of the specimen. In the case of the inflatable, the original height is the height of inflatable without an internal pressure ($35\,\mathrm{mm}$). The dimensions of the materials can be found in appendix A table 2. Some stress-strain curves were jagged due to the small specimen size or low stiffness, in combination with the '100 N' force sensor. In these cases a moving mean filter of window size 15 on the force samples is applied, see table.2. Although the linear actuator moves at a constant velocity and samples are taken at a constant rate, a moving mean filter of window size 15 is used on the distance samples to account for irregularities in the distance sensor or actuator speed. The last 20 samples, when the actuator decelerated ($2\,\mathrm{s}\cdot 10$ samples/s), are omitted for the inflatable since the force decreases at this moment (likely due to viscosity). For the other variations the last 5 samples are omitted since these gave unexpected values. For the Inflatable, the distance from the compression plate to the initial height of the inflatable ($35\,\mathrm{mm}$) was measured to calculate the strains. For the other backings a force threshold value was used to dictate the start of compression strain. This threshold is twice the resolution of the used force sensor ($0.01\,\mathrm{N}$ or $0.1\,\mathrm{N}$).

The Hydrogel specimens were tested directly after cooling down for $3\,\mathrm{h}$ in the refrigerator since they lost water content with time.

2.3.3 Backing: preload contact stress distribution

The contact stress distribution characteristic of the backings, under a preload, is measured with a preload sensitive film in between the backing and contact surface. The backing is compressed between a curved surface, the same as the curved substrate used in the experiment (sec.3) and flat surface, since the preload in the experiment is applied with a flat panel. Contact stress is measured at both ends of the backing (the preload application side and substrate

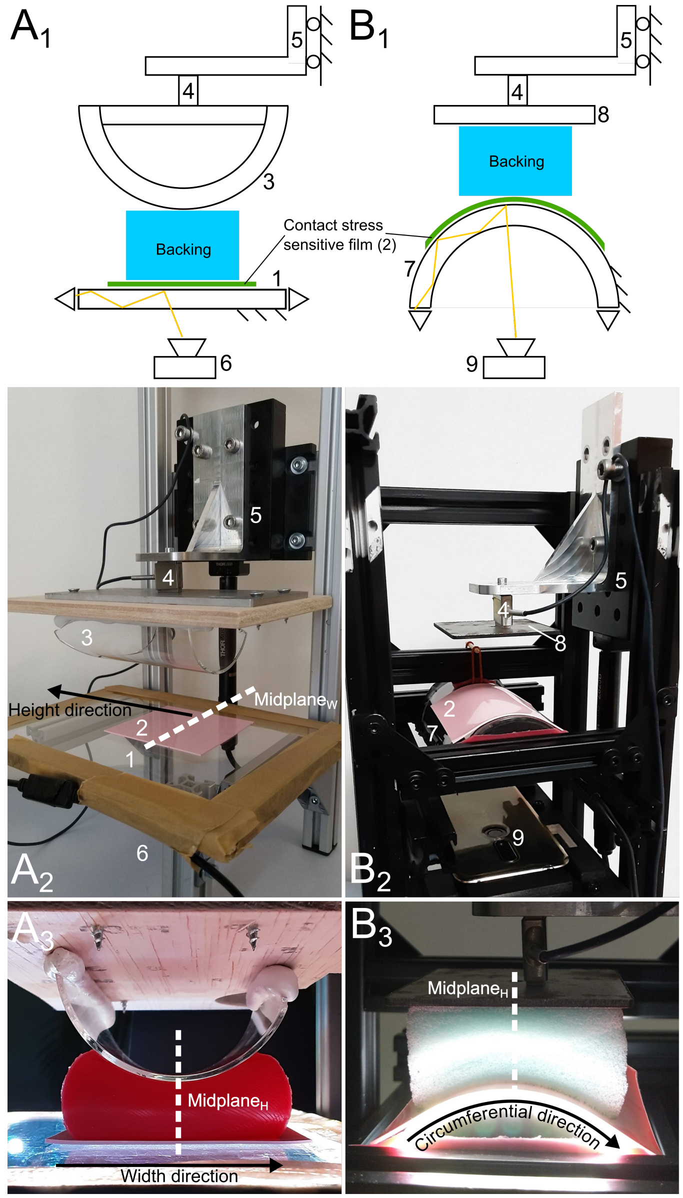

Fig. 9: Setups used to measure the contact stress of a backing on a flat substrate and a curved substrate. A1: Schematic of setup used for the flat substrate. A2: setup for the flat substrate (1). Into the substrate shines a LED strip attached with brown tape. Scattered light from the preload sensitive film (2) is captured by a bottom-view camera, located at (6). A cylinder (3) with the same outer diameter as the curved substrate is connected in series with a force sensor (4) and linear actuator (5). A3: Backing S-20/14 compressed 50% at the midplane$_\mathrm{H}$. The width direction of the captured images is indicated. B1: Schematic of setup used for the curved substrate. B2: setup for the curved substrate (7). The film (2) rests on top the curved substrate (7). A LED strip is taped to the sides of substrate (for more detail see fig.15A). Below the glass surface is a camera (9). A backing is placed between the film and a flat plate (8). The plate is in series with the force sensor (4) and linear actuator (5). B3: Backing P-S compressed 50% at the midplane$_\mathrm{H}$. The circumferential direction of the captured images is indicated.

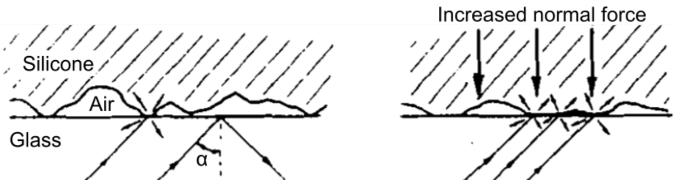

Fig. 10: Contact stress distribution measurement principle. When the incident angle α is great enough, light traveling through the glass is internally reflected at the glass-air interface. Reflection can not occur at the glass-silicone interface since the refraction index of silicone is higher than that of glass, and light is scattered at the interface. Under an increased normal force more silicone asperities come into contact with the glass to carry the load. The amount and locations of scattered light correlate therefore to contact stress. Adapted from [47].

side). Two combinations of substrate and preload object are used for this: One, the curved substrate in combination with a flat plate (see fig.9A1), and two, a flat substrate in combination with the curved 'substrate' as preload object (see fig.9B1). The film in combination with the frustrated internal reflection method (FTIR) produces, depending on contact stress, different light intensities coming from the contact area. Conversion measurements were done to find the relation between light intensity and contact stress for each film. However, the measured light intensity range in the conversion measurement was found to be smaller than measured light intensities of some backings. Still, due to the positive relation between light intensity and contact stress, light intensity is presented in the results as proxy for contact stress. The results should therefore be taken qualitatively instead of quantitative. Therefore the contact stress, with light as proxy for contact stress, is referred to as the 'contact stress', and the distribution as the distribution characteristic. First, the 'contact stress' measurement with FTIR is explained, then the light intensity to contact stress conversion measurement, and lastly, the data analysis of the light intensity that is a proxy for contact stress. For all backing design concepts one or two backing type variations are chosen to gain an impression in the contact stress distribution of their design concept: one solid, S-20/14, one open and one closed Inflatable variation to also compare the open and closed variations, I-O2 and I-C2, one sponge, P-S, and both rigid variations to check their conformability to the substrate with similar shape, R-C and R-F.

2.3.3.1 'Contact stress' measurement by FTIR:

The normal preload acting on one side of the backing is transferred through the backing to the other side that connects to the adhesive. The distribution of this preload onto the adhesive side is measured with a preload sensitive film. This film is a $1\,\mathrm{mm}$ thin soft (silicone) slab with a smooth surface and a rough surface, since it is poured onto sandpaper (see apx.A fig.23). Two different films are used. The first is called 'S40G180', made with (transparent) silicone of shore hardness 50A (Silicone elastomer, Sylgard 184) on 180 grid paper (3M SandBlaster 180 fijn) with 5 wt% pink pigment added (silicone pigment pink, Siliconesandmore). The second film is called 'S8G600': (pink) silicone of shore hardness 8A (softer than shore 50A) on 600 grid paper (GAMMA schuurpapier watervast fijn K600) with 5 wt% white pigment added (silicone pigment white, Siliconesandmore). The film is compressed between the backing and substrate, and the rough film side faces the substrate.

When the preload increases, an increasing amount of roughness asperities comes into contact with the substrate and their total contact area increases, which can be measured (with FTIR [47]), see figure 10. This increase of contact area of the asperities with increased preload (normal load) rests on the basis of a constant friction coefficient. Frictional forces scale linearly with real contact area between surfaces, and, taken that a surfaces has a multiscale roughness, the relation between real contact area and normal load is linear [48]. Since most surfaces have some arbitrary/hierarchical roughness, which makes it a multiscale surface, their friction coefficient is constant. However, surface asperities will deform under a load, and, when the normal load is high enough the surface is flattened, making the friction coefficient not constant [49]. The basic of dry adhesion systems is that the surface is not multiscale or that the normal load to flatten the surface is low. When the roughness or stiffness of a surface increases, the load 'threshold' is higher at which true contact area does not scale linear anymore with normal load [49].

The substrates used are from glass and Polymethyl methacrylate (PMMA), such that light can travel trough it. Light is radiated from a LED strip from the sides of the substrate, see figure 9A1,B1. The light traveling trough the glass is totally reflected within the glass when its incident angle with the glass surface is large and the medium in contact with the glass has a lower refractive index than glass. When a medium with a similar or higher refractive index, in this case the silicone asperities, is in contact with the glass, the light is not internally reflected but scattered, see figure 10. This method reveals also asperities that are within a few hundred nanometers ($300\,\mathrm{nm}$), due to the evanescent wave of the light [50]. The scattered light coming from the contact areas are picked up by a camera. In supplement movie 2, the film S40G180 is shown while increasing the applied preload (normal load). The time in this video is linear with the preload magnitude. It demonstrates that under increasing preload, more asperities come into contact, contact points can become larger, and there is an increase of light picked up by the camera. Contact areas on round surfaces have been measured using this method (soft gripper on tube [26], frog on solid cylinder [51]), but to the best of the knowledge of the author no contact stress distribution. When the asperities are pressed on the curved substrate, there may be shear contact stresses, besides the normal contact stresses, that will deform the asperities. It is expected that these shear forces will not make the surface flat, such that the surface keeps its multiscale property. With this assumption the method measures only the normal contact stresses.

The backings are compressed between a cylindrical surface and a flat one. The pressure distribution is measured on both sides, each with a different setup, by placing the film on either the flat PMMA substrate (fig.9)A2 or the curved glass substrate (fig.9B2). An image is taken when a soft backing is compressed to 17% and 50 % from its original height at the midplane$_{\mathrm{H}}$, and for a rigid backing when the film is compressed for $0.2\,\mathrm{mm}$. These values are somewhat arbitrarily chosen, but give an indication for low compression strains and high compression strains for the soft backings. The planes and orientations are defined in figure 9). In figure 9A3,B3 the backings S-20/20 and P-S are shown at a compression of 50% at the midplane$_{\mathrm{H}}$. The image of the curved substrate is a distorted image of the contact plane and is therefore mapped to a flat plane with the Matlab functions: 'fitgeotrans' (option: 'lwm','12') and 'cpselect' (with 100 control points)(see apx.B fig.27). The control points, identifying the same spots of the distorted image in a flat plane, were made by laying a paper with $5\,\mathrm{mm} \times 5\,\mathrm{mm}$ grid on the curved substrate and on a flat plane (apx.B fig.28A-D).

2.3.3.2 Conversion measurement:

The conversion from light intensity to contact stress is measured by varying the mean preload stress and measuring the resulting mean light intensity over the projected contact area. The projected contact area is the region on the film below the object's surface that preloads the film. The mean preload stress is the preload divided by the projected area. The conversion is dependent on: the film's roughness and softness, the light source intensity, and the light settings of the camera. The conversion for the flat substrate was measured by compressing the film with another flat surface, and for the curved substrate by another curved surface, the curved side of R-C (see apx.A fig. 24). R-C has a slightly larger diameter as the top side (smooth side) of the film when it sits on the curved substrate. This is since the film is $1\,\mathrm{mm}$ thick and R-C was made by casting it onto a $2\,\mathrm{mm}$ thick adhesive that sat on the curved substrate (see for manufacturing sec.2.2.5) In both conversion measurements a sponge is used between the smooth side of the film and preload object to account for misalignment and surface irregularities. The conversion was measured for both films on the flat substrate and for one film (S40G180) on the curved substrate.

The rough side of film S40G180 has a rougher surface than film S8G600 since it is poured on sand paper with a lower grit size. This implies that S8G600 has a more fine distribution of asperities and therefore resolution. However the maximum preload to which S8G600 can be used is lower than S40G180. This is because the rough surface of S8G600 is easier pressed flat than S40G180, due to its lower roughness and softness [49]. For the higher resolution film, S8G600, the preload up to which the conversion is measured is $10\,\mathrm{N}$ for a projected contact area of $5\,\mathrm{cm} \times 5\,\mathrm{cm}$, resulting in a mean preload stress limit of $4\,\mathrm{kPa}$. For the lower resolution film, S40G180, the preload up to which the conversion is measured is $45\,\mathrm{N}$ for a projected contact area of $5\,\mathrm{cm} \times 5\,\mathrm{cm}$, resulting in a mean preload stress limit of $18\,\mathrm{kPa}$.

The film S8G600 is preferred due to its resolution, and is used on the flat substrate for the inflatable, sponge, and rigid. The film S8G600 on the curved substrate gave light saturation of the camera, due to the higher light source intensity on the curved substrate setup. Therefore the film S40G180 is used on the curved substrate for the inflatable, sponge, and rigid. Due to the stiffer nature of the solid, needing a higher preload at a 50% compression, the film S40G180 was used on both the flat and curved substrate for the solid since the conversion values of this film seemed linear over a greater mean preload stress range than that of S8G600 (apx.A fig.25.

The lowest possible camera (Nokia 7.1, setting; ISO 100) shutter time (1/500 s) was used for S8G600 since a higher shutter time gave more light saturation, the same holds for S40G180 on the curved substrate. For S40G180 on the flat substrate a longer shutter time (1/60 s) was used to increase the absolute light intensity differences over the contact area in the contact stress distribution characteristic.

In all resulting conversion measurement (see apx.A fig.25) the relation between mean light intensity and mean preload stress is a monotonically increasing one. The softer film S8G600 sticks a bit to the flat substrate giving a higher mean light intensity at no preload right after removing the maximum load, compared to the start of the preload.

2.3.3.3 Data analysis:

To make the trends seen in the captured contact stress distribution characteristic images more clear, the effective pixel size of the images is reduced. This is needed since the films have a certain 'asperities resolution'. Since film S8G600 was cast on a finer grid sandpaper the image pixels are reduced to 402×402 and the images of film S40G180 to 121×121 pixels. For a captured area of $6\,\mathrm{cm} \times 6\,\mathrm{cm}$ this gives an effective pixel width of $0.15\,\mathrm{mm}$ and $0.5\,\mathrm{mm}$ respectively.

Light intensity at the effective pixel size is calculated by averaging the light intensity of the original smaller pixels, which have discrete values between 0 and 255.

The conversion measurement of film S8G600 gave a maximum mean light intensity of 24, and for the film S40G180 on the curved substrate gave a maximum mean light intensity of 105 (apx.A fig.25). The maximum measured light intensity in the measured backing contact stress distribution characteristics, lie around 50 for S8G600 and around 200 for S40G180. This means that the conversion values measured did not span the light intensity range found with the backings contact stress distribution characteristics. Therefore, the light intensity is not converted to contact stress.

Due to the decrease of mean light intensity with mean preload stress (apx.A fig.25), the maximum contact stresses are underestimated. Thus the real contact stress distribution would be more pronounced.

The 'contact stress' is presented in two ways. The first is of the whole contact area. In the second, a cross-section of the image is taken along the midplane$_{\mathrm{W}}$. This cross-section is made by taking the average light intensity of the middle third pixel rows in the height direction, with the midplane$_{\mathrm{W}}$ in its center. This corresponds to a band of $2\,\mathrm{cm}$ wide. This band fits between the bright corners found in figures 12B1,B3.

Since the backings on the curved side were measured with the same film (S40G180) and light settings, the light intensity values between the backings on the curved side are comparable. On the flat side, the Inflatable, PUR-sponge, and the Rigid variations, use the same film (S8G800) and settings. Silicone on the flat side uses the film S40G180 (and its light intensity is thus incomparable with others).

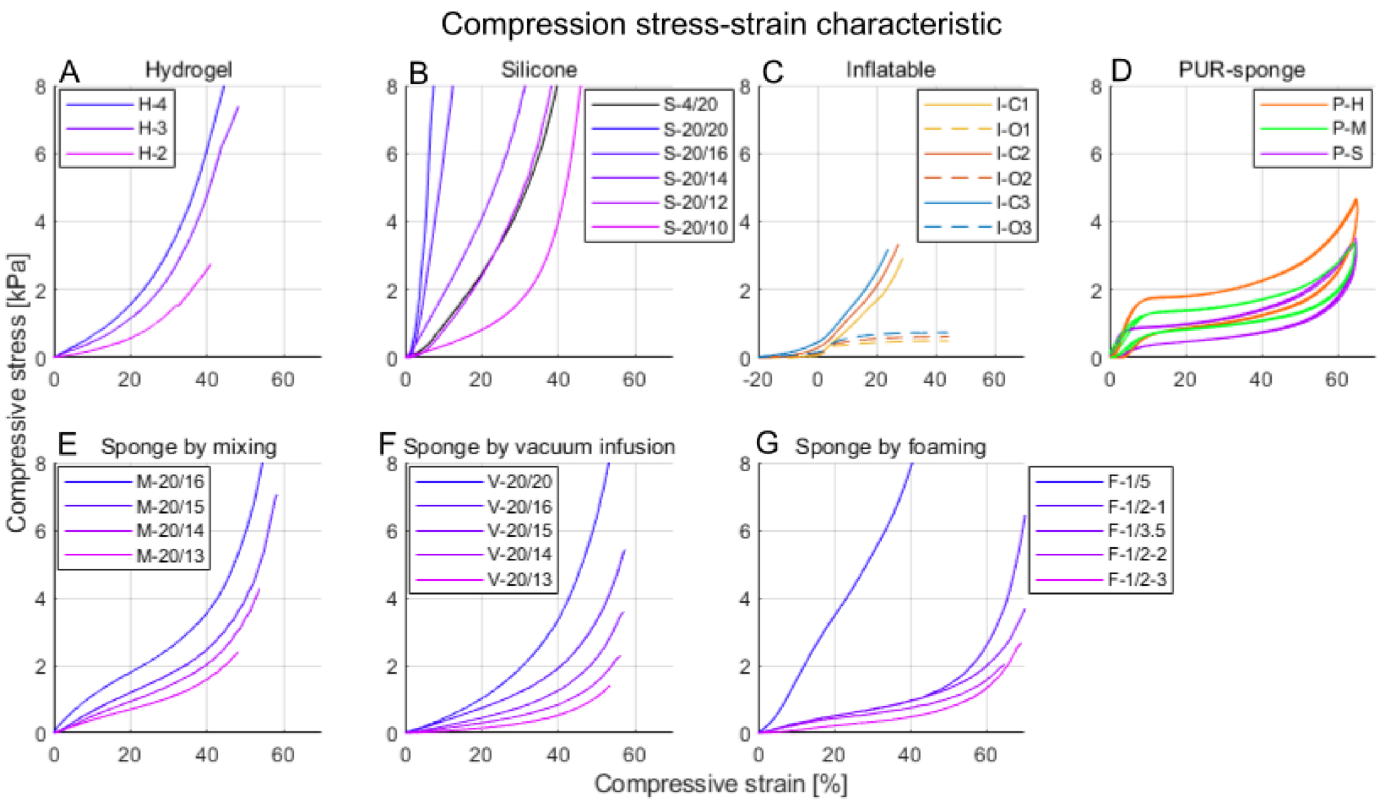

Fig. 11: Compressive stress of the backing variations as a function of compressive strain. The Hydrogel (A) gets softer with decreasing gelatin content. The Silicone (B), Sponge by mixing (E), and Sponge by vacuum infusion (F), get softer when the parts 'a' to parts 'b' mixing ratio of their silicone constituent increasingly differs from the standard 20/20 ratio. The inflatable (C) has a negative strain since its height expands when pressurized. The PUR-sponge (D) is plotted during the compression stroke and on the return stroke.

2.4 Characterization results

The results of the characterization measurements are summarized in table 1.

2.4.1 *Adhesive: frictional load capacity*

The load versus distance curves of the adhesive showed an increase in load up to a maximum and afterwards a lower and slowly declining load (see apx.B fig.29A). At the end of a measurement of an adhesive, the adhesive had slid on the substrate and its contact area did not visually change much. Thus, the contact area of an adhesive at the maximum load and during sliding was in both instances $\approx 25\,\mathrm{cm}^2$. With this surface area the load capacity per surface area of the adhesive is estimated.

The maximum load measured, the maximum load capacity of the adhesive, for the 'variability measurement' between adhesives, M_{Av}, and for the 'repetition measurement' of one adhesive, M_{Ar}, are (mean 53.3, std 5.5) and (mean 47.1, std 1.3) respectively. The load at the end of the slide, the slide load capacity, for the 'variability measurement', S_{Av}, and for the 'repetition measurement', S_{Ar}, are (mean 33.4, std 1.1) and (mean 33.5, std 1.6) respectively. The relative variability, of two standard deviations from the mean to the mean, for M_{Av}, S_{Av}, M_{Ar}, and S_{Ar}, are 0.21, 0.07, 0.06, and 0,10 respectively.

2.4.2 *Backing: compression stress-strain characteristic*

The measured stress versus compression curves are shown in figure 11. From these stress-strain relations, compression moduli (stress/strain) were calculated at 17% and 40%, see apx.A fig.22. In table 1 the range of compression moduli is noted. This range is noted as the lowest compression modulus at 40% and highest modulus at 40%. When the highest modulus was not available at 40%, it is noted at a lower maximum measured strain. This maximum strain limit was due to either, a backing material was too stiff for the force sensor's force limit, or the actuator's displacement limit.

The Hydrogel becomes softer with decreasing gelatin content, see figure 11A. The Silicone, Sponge by mixing, and Sponge by vacuum infusion, get softer when the parts 'a' to parts 'b' mixing ratio of their silicone constituent increasingly differs from the standard 20/20 ratio, see figure 11B,E,F. The inflatable is stiffer, over the whole measured strain domain, when the initial inner pressure is higher, see figure 11C. A closed inflatable is stiffer than an open inflatable with the same initial pressure. For a closed balloon the stiffness increases with increasing compression, while for an open one the stiffness decreases. The inflatable has a negative strain since its height expands when pressurized, and the initial height is the height of the non-pressurized inflatable. The modulus of P-S, at both compression strains, either in the compression stroke or return stroke, is smaller than that of P-M which is smaller than that of P-H. The PUR-sponges show a hysteresis curve in which they experience a smaller stress on the return stroke, see figure 11D. For a PUR-sponge the stiffness first decreases with increasing compression, and later increases. The 'Sponge by foaming' variation F-1/2-x specimens, have different compression moduli although their constituents are the same. The curve of the F-1/3.5 specimen lies in between those of the F-1/2-x specimens while it has different constituents, see figure 11G.

The Hydrogel specimens fractured during the measurement. H-2 did so first, around 30% strain, which was seen by the small dip in its curve. Even with the foil to displace the Hydrogel specimens, some cracks formed during transportation.

Also plotted in figure 11B is the Silicone variation S-4/20 (represented by the black curve). This is the material used as adhesive material for the adhesive.

2.4.3 Backing: preload contact stress characteristic

Here the results are presented of the contact stress distribution measurement. Figures 12B,C,D were made with the same settings, thus light intensity refers to the same absolute units, figure 12A has different settings. In figure 13 the subfigures of the curved substrate use the same settings, the subfigures of the flat substrate use the same settings with the exception of the solid (fig.13A2), which uses again different settings.

General trends in contact stress distribution characteristics on the curved substrate are (fig.13A1,B1,C1,D1): Peak contact stresses were found with the rigid backings and for the inflatable specifically under the contact edge and in the center. Compared to the latter, the sponge and solid, at the smaller compression (maximum compression strain of 17% along the midplane$_H$), had a more even distribution. At the higher compression (maximum compression strain of 50% along the midplane$_H$), the solid's contact stress became relatively higher in the center while the sponge kept a more even distribution. Furthermore, the contact width of the solid, inflatable, and sponge, increased with compression.

General trends in 'contact stress' on the flat substrate are (fig.13A2,B2,C2,D2): Peak contact stresses were found with the rigid backings and, at the higher compression, at the contact edges of the solid and inflatable. Compared to the latter, the solid, inflatable and sponge, at the lower compression, showed smaller peak stresses. The sponge kept a similar even stress distribution at the higher compression.

Besides the general trends mentioned for the inflatable, some specific results are noticed. Starting with contact with the flat substrate, the contact stress along the midplane$_H$ (fig.13B2) can be divided in three regions. The contact edges where peak stresses occur at high compression, a region besides the edges where no stress occurs, and a center region where stresses are relatively even. The stress in the center region, of the open Inflatable (IO-2) on the flat substrate, is relatively unaffected by compression depth (fig.12B1,B2)(fig. 13B2). At the edges, stress does increase with compression (fig. 13B2). With the closed Inflatable (IC-2) on the flat substrate, the stress increases with compression depth, not only at the edges but also in the center region. Furthermore, on the flat substrate, the stress at the edges is higher for I-C2 than I-O2 at high compression. On the curved substrate. The inflatable shows higher stress in its center and at the contact edges. These contact edges lie under the walls of the inflatable I-O2 but not for I-C2 since the contact width in the latter is approximately $4\,\mathrm{cm}$.

The sponge shows some overlap of its stress distributions on the curved substrate, between low and high compression, at a circumferential position of around $15\,\mathrm{mm}$ and $40\,\mathrm{mm}$ (fig. 13C).

The 'Sponge by mixing' variation M-20/16, at high compression on the flat substrate, shows some small regions of no stress and at all edges a relatively higher stress (fig. 12C1). The 'Sponge by vacuum infusion' variation V-20/20, at high compression on the flat substrate, has higher stress in its center (fig. 12C2).

The Rigid curved variation R-C does not make full contact with curved substrate (fig.12A5), neither does the flat variation R-F on the flat substrate (fig.12D).

2.5 Discussion design

In this section the backing design concepts, characterization methods and fabrication are discussed. The discussion ends with choosing suitable backing types, and fabrication of the resulting adhesive systems that are used in the experiment of section 3.

2.5.1 Backing design

In the next subsection the behavior of the rigid, solid, inflatable, and sponge backing design is discussed. The behavior includes the found characteristics of their compression stress-strain characteristic and contact stress distribution characteristic under preload. From these characteristics some conclusions are drawn with respect to the design objectives for a backing. In the conclusion (sec.4) there is a reflection on the biological backings.

2.5.1.1 Rigid:

The Rigid curved variation R-C does not make full contact with curved substrate (fig.12A5). This could be explained by how the variation was made. R-C was made by pouring polyester onto an adhesive attached to the curved substrate. This adhesive is $2\,\mathrm{mm}$ thick while the pressure sensitive film is $1\,\mathrm{mm}$ thick. However, the combination of R-C with the adhesive, R_S-C, did not make full contact either with the curved substrate in the experiment (apx.B fig.30). The flat variation R-F on the flat substrate did also not make full contact (fig.12D). Both these cases support the idea that a rigid backing design will not be perfect enough to conform exactly to the substrate if that would have the same shape, and also here a soft backing would be preferred.

2.5.1.2 Solid:

The contact stress distribution characteristic of the solid on the curved substrate at low compression was relatively even, compared to the other backing designs (fig.13A1,B1,C1,D1). This could indicate that a Solid might prove as useful backing design to distribute the preload at small compressions. This is unexpected since its stress-strain characteristic shows an increasing stiffness with strain.

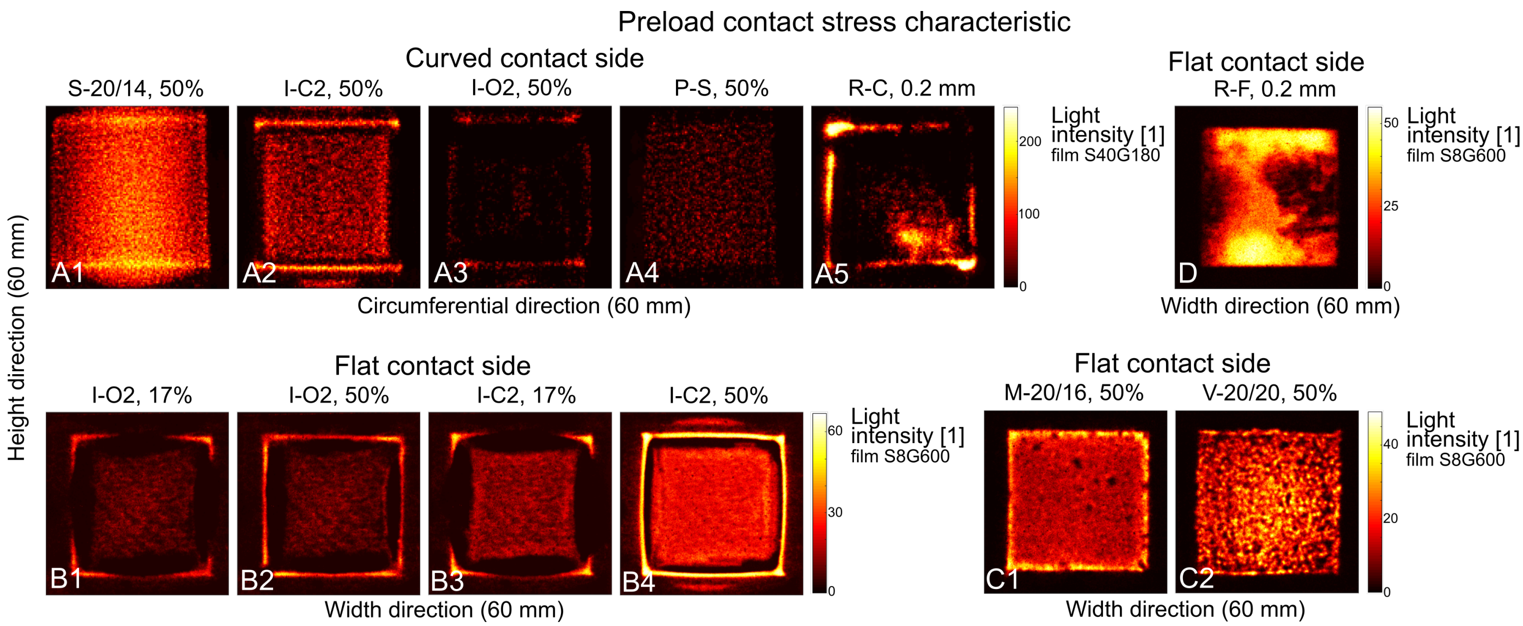

Fig. 12: Contact stress distribution characteristic of backings pressed on either the flat or the curved substrate. The measured light intensity functions as proxy for contact stress. Light intensity is positively related to contact pressure. Pixel width is 0.5 mm in A and 0.15 mm in B-D. The colorbar refers to the light intensity of an effective pixel. B, C and D were made with the same settings, thus light intensity refers to the same absolute units, A used different settings. (The height, width and circumferential directions are indicated in fig.9.)

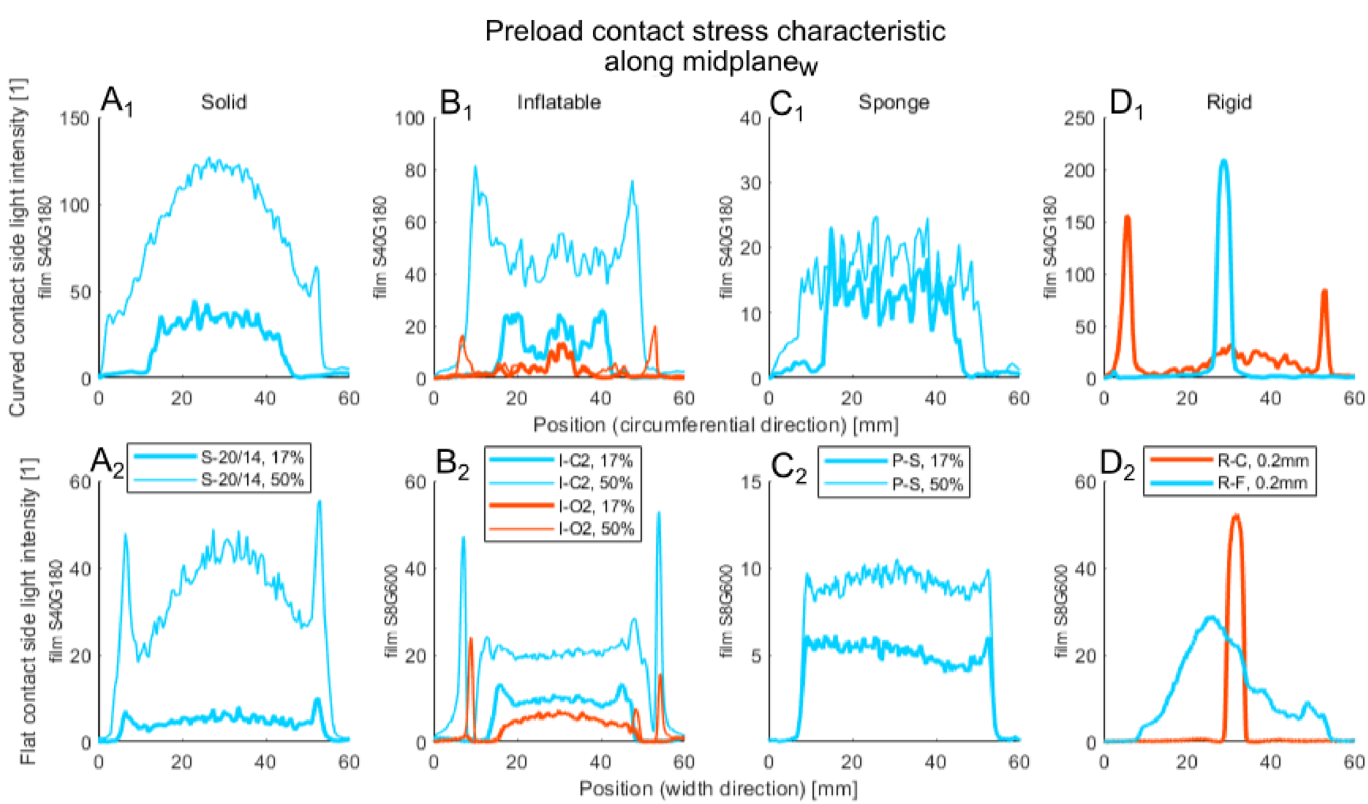

Fig. 13: Contact stress distribution characteristic cross-section along the midplane$_W$. The percentages stated after the backing names refer to the compression percentage at their midplane$_H$. (The midplane$_W$ and midplane$_H$ are indicated in fig.9.)

The characteristic on either the flat or curved substrate was more even at low compression compared to high compression (fig.13A). This could be due to the exponentially increasing stiffness with strain, which increases differences in stress in a strain interval.

Due to its solid nature, the Silicone backing type will expand laterally when compressed. The stress concentrations at the contact edges for the solid S-20/14, on the flat substrate at high compression, might come from this lateral expansion while simultaneously the contact edge is stuck due to friction. The Hydrogel and Silicone show an exponentially increasing stress-strain curve. This increase could be due to the increased cross-section with compression. However, it is likely the case that the polymer chains rearrange from a random shape to a straight one and thereby increasing the stiffness at higher deformations.

2.5.1.3 Inflatable:

The fabricated Inflatable showed that the inflatable design helps to reduce the softness of the backing compared to a solid design. Also, the open variations are softer than the closed variations as expected.

It was seen that for a closed Inflatable the stiffness increases with strain, while for an open Inflatable the stiffness decreases. Due to the constant internal pressure for the open Inflatable, the initial higher stiffness of the open Inflatable, can therefore be attributed to the wall stiffness, which likely decreases with increasing strain due to buckling of the walls.

The case was made that the internal fluid helps distribute contact stress more evenly since the pressure in the fluid is even. Now the case is made that internal fluid is more of a hindrance since the fluid will always have to be contained by some hull. In the contact stress distribution characterization of the Inflatable under a preload on a flat substrate the following was found:

On the flat substrate the Inflatable showed peak stresses at the contact edges. Since the contact width was $5\,\mathrm{cm}$ here, the contact edges correspond to the location under the Inflatable's walls. Indicating that the preload is relative more transferred through the hull of the Inflatable. At the flat contact side, the stress under the walls is higher for I-C2 than I-O2 at the same compression, which means that the effective wall stiffness is dependent on internal pressure. The center contact region does have a relatively even contact stress distribution. On the flat substrate I-O2 keeps in the center region a constant contact stress from the smaller to higher compression, but contact stress increases at the edges with compression. This suggests that the walls have no effect on contact stress in the center. Some of the contact stress that does occur in the center region could be explained by gravity. However, for the flat side of I-C2, the contact stress, at small and high compression, is higher in the center region than I-O2 at the same compressions. This suggests that a higher internal pressure presses on the center region, causing higher contact stresses. Although this indicates an even contact stress distribution due to the fluid, in the center region, this is likely an artifact of the flat on flat contact the Inflatable made with the flat substrate. This artifact could come from the flat shape of the hull sides when un-inflated. Taken that an un-inflated inflatable compressed on the flat substrate would experience no contact stress in the center contact region; and when this un-inflated inflatable is then pressurized, the pressure would exert an even stress on the center region. The pressurization would also push on the walls which in turn want to bulge outwards, rotating the contact edges. This rotation would lift up the contact area beside the walls, and this could explain the 'no stress region' next to the contact edges. Although the air has the same pressure everywhere, the Inflatable does not have an equal contact stress on the curved contact side. There were peak stress at the contact edges and center region. This is most likely due to the hull. Therefore, it is concluded that internal pressure is needed to have contact pressure in the center (between the wall edges) for instances where the inflatable has the same shape as the substrate (when the contact edge is stuck). But that in other instances the contact stress depends on the deformation the hull has to make, and is therefore, not an even stress distribution. (fig.13B1). An equal contact stress distribution with an inflatable is therefore in most cases not the case. Furthermore, the internal pressure will only change the initial outer shape and increases stiffness of the inflatable [26]. The conformability of the inflatable and the resulting contact stress is therefore guided by the hull's shape [52].

On a curved substrate the Inflatable did not give a higher total contact area or a more even contact stress distribution characteristic than a solid or sponge, (fig.13A1,B1,C1).

When the internal overpressure is omitted in an open Inflatable to reduce stiffness and complexity, the open Inflatable can be considered an open celled sponge, with one cell.

2.5.1.4 Sponge:

The fabricated silicone sponges showed that the sponge design helps to reduce the softness of the backing compared to a solid design.

The compression stress-strain characteristic of the PUR-sponge shows an initial high slope and subsequently a plateau. The initial slope is related to the relatively low softness of PUR, and the plateau is caused by the buckling of the sponge's cell walls [46]. This plateau causes the sponge to be relatively soft at higher strains. It was expected that a material with a 'plateau' in their compression stress-strain characteristic, such as the sponge, will produce a more evenly distributed contact stress, since the stress in the material will be similar for a large range of deformations. This is exemplified by the overlap of the stress distribution characteristic of P-S on the curved substrate, between low and high compression (fig. 13C1). As expected, the contact stress characteristics of the PUR-sponge had a relatively even distribution, at low and high compression, on both the flat and curved substrate.

The stress-strain characteristics of the silicone sponges M-x/x and V-x/x do not show a decreasing stiffness up to 40% compression like the PUR-sponges do. This could be due to the higher component of silicone (60 v%) compared to PUR (>90 v%) in the sponge. Resulting in thicker cell walls in the silicone sponges which do not buckle.

When the preload on an adhesive system is removed, the backing will inevitably balance compression forces with tension forces implied by the deformation. Cell walls in tension do not buckle and the sponge loses the buckling effect mentioned. Keeping in mind that a contact stress after preload without peak stresses is a design objective, materials with a non-linear stress-strain behavior in tension can be investigated for this purpose. Contact stress distribution under tension can not be measured with the method here but an adaptation, by using underpressure between the film and substrate, can be used [53] or computational methods.

2.5.2 Characterization methods

The methods to measure, the compression stress-strain characteristic and compressive contact stress, are discussed. For the setup and discussion of the method used to measure load capacity of the adhesive see section 3.

2.5.2.1 Compression stress-strain characteristic:

Caution should be used when comparing stress-strain curves of sponges with solids. Not only since only one specimen and measurement is used per variation, but also since solids expand laterally when compressed, increasing their cross-section. Also caution should be used when interpreting the stiffness slopes at the first percentages of strain, since some surfaces were rough and slanted.

2.5.2.2 Preload contact stress characteristic:

The measured conversions have a decreasing slope with increased mean preload stress (apx.A fig.25). This could be due to the film loosing its multiscale surface property at a too high preload. The decreasing slope could also be due to light saturation of the camera when more light is emitted from the film at a too high preload. Although not presented here, with a longer shutter time the slope decreases even faster with increased preload, indicating that shutter time increased light saturation in the camera and might have played a role.

For future preload/pressure sensitive films it follows that a finer grid of the sandpaper allows for a higher resolution, and a lower softness of the film will increase the range of stresses that can be measured. Shutter time and light source intensity should be adjusted to each other, i.e. high light source intensity to reduce background light requires a camera with a short shutter time. Furthermore, the maximum light intensity coming from the film should trigger the maximum pixel light value of the camera. This would give the light intensity the greatest resolution (1/256). Shutter time should be adjusted to this.

2.5.3 Fabrication

First the fabrication of the adhesive and backings is discussed. Later, the fabricated adhesive and backings are compared to the requirements stated at the start of this section. Taking fabrication difficulties into account, usable adhesive systems are presented at the end, including the bonding between adhesive and backing.

2.5.3.1 Adhesive:

When the silicone mixing ratio increasingly differed from the normal mixing ratio (20/20), the adhesive material felt subjective increasingly tacky. The Dahlquist criterion [11] explains that an adhesive's softness increases real contact area with a substrate and scales greater than the adhesive's work of adhesion, with respect to bond strength. Work of adhesion is the work required to separate a certain area of the interface between the adhesive and a perfectly flat substrate [11]. Thus the increased tackiness is likely due to increased softness with more uneven mixing ratio (fig.11B). Silicones with greater uneven mixing ratios than S-20/12, like S-20/10, became too brittle to handle. Mixing more parts 'b' than 'a' gave the Silicone variation S-4/20 (represented by the black line in fig.11B). Although S-4/20 is as soft as S-20/12, it was found that it is less brittle than S-20/12, making S-4/20 the preferred material for the adhesive material.

2.5.3.2 Backings:

Here, some difficulties and other noticed things are discussed of the Hydrogel, Inflatable, and silicone sponges.

Hydrogel proved brittle at strains around 30% which makes it likely unsuitable to deform around the curved substrate. Furthermore the Hydrogel lost water content with time and would be difficult to bond to the adhesive.

In supplement movie 1 about the open Inflatable, only a decrease of $0.5\,\mathrm{cm}$ of the water column in the the pressure sensor was seen, instead of the estimated $1.5\,\mathrm{cm}$. If this pressure drop was caused by a leakage, the pressure sensor would have returned to a different value. Thus, it is probably due to the elasticity of the air reservoir hull which gives more room for the air.

The higher compression stiffness of the 'Sponges by mixing' compared to the 'Sponges by vacuum infusion' is probably due to the higher relative sugar density of the latter (0.68 compared to 0.6). Sugar grains connected as a sugar cube are more densely packed compared to loose grains.

When mixing sugar crystals with an amount of silicone (0.15 v%) that was less than the empty volume between the crystals (0.4 v%), a hollow sponge formed (apx.A fig.20C). This could be due to the tendency of silicone to cluster at the outer surfaces. This could be explained by that silicone attracts silicone and its surface tension at the outer surfaces would be lower than in the center, and is therefore pulled there.

The black spots in the contact stress characteristic of M-16/20 on the flat substrate (fig.12C1) seem to correspond to the holes in its surface (apx.A fig.20I1,I2). The sponge M-20/16 was cut revealing a sponge structure within more solid edges which could explain the higher stress found at all contact edges (apx.A fig.20I1,I3). The edges are likely more dense since sugar crystal were less dense packed here due to the mould wall.

Of the larger vacuum infused sponges (V_x-20/13, V_x-20/14, and V-20/20) only V-20/20 kept the shape of the sugar cube (apx.A fig.20E). This was initially not noticed for the smaller samples (fig.20D). The sagging is likely due to

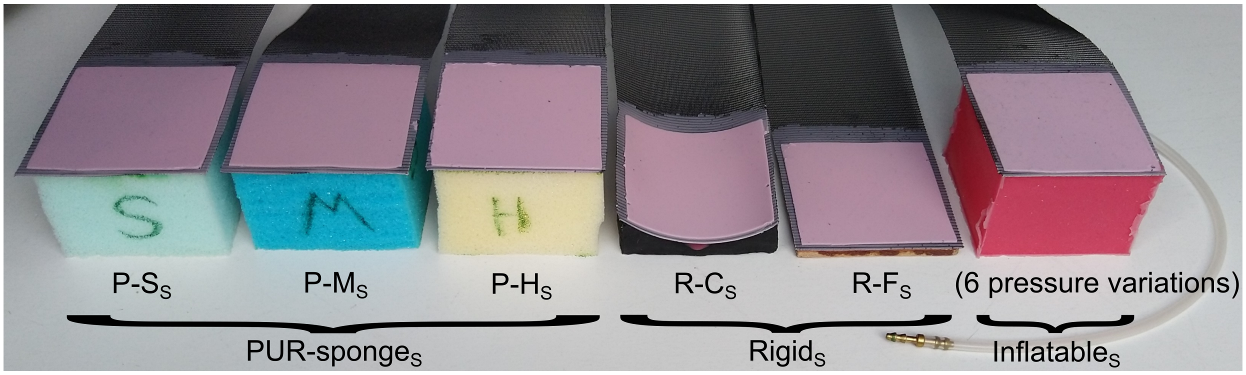

Fig. 14: Adhesive system types, with their variations, used in the experiment (section 3). The PUR-sponge system has three variations in softness: P_S-S, P_S-M, P_S-H. The Rigid system has two variations, one which is planar (R_S-F) and one where the adhesive surface has the same diameter as the substrate (R_S-C). The Inflatable system in conjunction with its air reservoir (shown in figure 6), can be pressurized to different internal pressures and also closed off via the silicone tube to make 6 variations: I_S-O1, I_S-O2, I_S-O3, I_S-C1, I_S-C2, I_S-C3. Dimensions of the PUR-sponges and Inflatable backing are $35\,\mathrm{mm} \times 50\,\mathrm{mm} \times 50\,\mathrm{mm}$. The adhesive is $50\,\mathrm{mm} \times 50\,\mathrm{mm} \times 2\,\mathrm{mm}$ with the tail of the reinforcing mesh sticking out for $20\,\mathrm{cm}$.

either or a combination of, its weight, low cell wall stiffness and stickiness of the silicone.

For V-20/20 a higher stress in the center region was noticed in the contact stress characteristic, at 50% compression on the flat substrate (fig. 12C2). V-20/20 has visibly a different structure in its core (see apx.A fig.20F). These two factors indicate a higher density in the core of the specimen. This happened probably due to the sugar cube being less dense in its core. The reduced sugar cube core density is likely an artifact of drying, whereby the core dried slower, allowing the damp water sugar mixture to diffuse/transport to the dryer outer parts and deposit there.

With the foaming fabrication method it was difficult to get consistent sponges. The cell sizes in a sponge also varied a lot. With an oven as heating element, the heating was not uniform in the sponge which gave difficulties making homogeneous sponges. But also with a (household) microwave heating was unexpectedly even worse, since big holes formed (see, apx.A fig.20F).

2.5.3.3 Fabricated adhesive systems:

Multiple backing types were made, 7 soft types and one rigid type. For all soft types it was shown that it is possible to make variations with a different softness. Not all backing types were suitable as the backing part for an adhesive system to be used in the experiment. Due to the impracticality and small elastic strain of the Hydrogel, the relatively high stiffness and weight of the Silicone and 'Sponge by mixing', and the difficulty of fabricating the 'Sponge by vacuum infusion' and 'Sponge by foaming', the following types were chosen as suitable backings: PUR-sponge, Inflatable, Rigid (Rigid variations are stiff but are used as control groups in section 3).

An adhesive was made that can keep full contact with the cylindrical substrate after removing the preload. The adhesive can do this multiple times. The reinforcement is relatively stiff to the adhesive material which theoretically implies that contact area(s) with the substrate are evenly loaded. Therefore it is suitable as the adhesive part of the adhesive systems to be used in the experiment.

With the chosen backing types and adhesive, adhesive systems were made, see figure 14. The names of the adhesive systems are those of the respectively backing type variation (e.g. P-S) with the addition of the subscript '$_S$' to indicate 'system' (e.g. P_S-S). To make an adhesive system, a backing is bonded to an adhesive over their whole mating surfaces (0.5 gram silicone, Resion siliconen gietrubber addition cure 8A, normal weight ratio part 'a' to 'b' 20/20). The adhesive specimens of the adhesive characterization were used.

3 Experiment

In this section an experiment was done to investigate the influence of the backing's 'softness', on the frictional performance of the adhesive system. The frictional performance is quantified by two parameters: the area of contact between the adhesive system and the substrate, and the frictional load capacity of the adhesive system.

Two studies are done, one on adhesive systems with a sponge backing, together with adhesive systems with a rigid backing as control group, and one with the system with an inflatable backing. The adhesive system types and their softness variations are shown in figure 14.

3.1 Experimental method

Here the experimental method is presented. Starting with the topology of the adhesive system and substrate, continuing with the independent variable 'softness', the dependent variables 'contact area' and 'load capacity' and the constant 'preload'. It finishes with the test routine, consisting of a 'preload phase', a 'rest phase', and 'load phase', test order of the adhesive system specimens, and data analysis.

3.1.1 Shape of substrate and adhesive system

Explained here is the choice of a suitable existing adhesive type, a curved substrate's shape that allows a high frictional performance of the adhesive, and chosen dimensions.

In this study the effect of the backing on contact with substrate macro undulations (shape) is investigated. Therefore, the adhesive should be relatively thin compared to the substrate macro undulations. This would imply that the adhesive can only make contact with micro undulations (roughness) of the substrate. For the backing to have effect on the contact made with macro undulations (shape), the backing should have dimensions at least in the same order as the substrate's shape.

This research is focused on the backing and therefore an existing adhesive will be used. To notice effects from the backing on load capacity with contact area, an adhesive is needed that is loaded evenly over its whole adhesive surface. Since for such an adhesive a linear relation between contact area and load exists independently of the contact area shape. Therefore, based on the adhesive of Bartlett et al.[7], the adhesive used is a thin planar soft adhesive material with a planar thin reinforcement, such as in figure 1A2.

The frictional performance of the adhesive system is limited by the frictional performance of the adhesive. Contact area should be maximized and internal stresses minimized. Therefore, the adhesive used here is thin and planar of structure. Such a structure has a low stiffness in bending but not in extension or compression (before buckling). Furthermore, the adhesive surface is smooth.

For substrates with undulations in multiple directions a planar adhesive has to stretch and compress, which results in internal stresses that can decrease the frictional performance of the adhesive substantially compared to its performance on a flat substrate. Especially if the tenacity (load capacity per surface area) of the adhesive is low compared to the induced internal stresses, contact area might end up to be to low to notice differences between adhesive systems with small samples sizes.

When a thin planar adhesive forms over a substrate with undulations in one direction, it only has to bend. Internal stresses will then be relatively low compared to the tenacity of the adhesive, which makes it more likely the adhesive stays stuck. Furthermore, in this study the preload has one degree of freedom, an up and down motion. Thus, even when there are undulations in only one direction, it is likely that the adhesive will touch the peaks of the undulations first, stick there, and will have to be stretched to make more contact in the 'valleys'. Therefore, a cylindrical substrate is chosen, where the adhesive only has to bend in one direction and over one undulation peak.

A cuboid shape is taken for the backings. It was chosen to have the height of the backing ($35\,\mathrm{mm}$) equal the radius of the curved substrate. The substrate is shown in figure 15B). The width ($50\,\mathrm{mm}$) of the backing is chosen as smaller than the diameter of the substrate, since the contact slope along the cylinder increases to $90°$ which makes contact unlikely at the outer contact regions. Furthermore, the depth of the backing was taken the same as the width of the backing ($50\,\mathrm{mm}$). The adhesive has an adhesive surface area of $5\,\mathrm{cm} \times 5\,\mathrm{cm}$, is connected with the opposite side to the backing, and has its reinforcement sticking out for $20\,\mathrm{cm}$.

3.1.2 Softness

Softness is the independent variable in this study. In this section the adhesive systems are presented with their softness variations shown in figure 14. Also, it is explained why the compression stress-strain characteristic (compressive stiffness) of a backing is used as general proxy for softness.

Three adhesive systems are used for the experiment; A system with a PUR-sponge as backing, called 'PUR-sponge$_S$', a system with the Inflatable as backing, called 'Inflatable$_S$', and a system with a rigid backing (as control group), called 'Rigid$_S$'.

To vary softness for the PUR-sponge$_S$, three variations of the backing type 'PUR-sponge' were bought. These backing variations are called P-S (PUR-sponge soft), P-M (PUR-sponge medium), P-H (PUR-sponge hard), and their compressive stiffness was measured in section 2, see figure 11D. The names of the adhesive systems are those of the respectively backing type variation with the addition of the subscript '$_S$' to indicate 'system': P_S-S, P_S-M, and P_S-H. The Inflatable$_S$ has 6 softness variations, namely, it can be in an open and closed state and is in both states pressurized to either 100, 200, or 300 Pa. In the open state the air inside the inflatable can escape and the pressure inside the inflatable is constant, these variations are called: I_S-O1, I_S-O2, I_S-O3. In the closed state the air inside the inflatable can not escape, these variations are called I_S-C1, I_S-C2, I_S-C3. The 'O' and 'C' in the names refer to the open or closed variations and the 1-3 to the initial overpressure (100-300 Pa). The compressive stiffness of the Inflatable$_S$ variations was measured in section 2, see figure 11C.

Since the system has to conform to a cylindrical substrate to make contact, it has to bend. Bending stiffness is dependent on the elastic moduli, and the same holds for the compressive stiffness (although they might differ in the strain values and elastic moduli involved). Therefore, and because the test is more common and convenient, the softness of a backing will be defined by their compressive stiffness. To know for sure whether a material with a lower compressive stiffness is also the one with a lower bending stiffness, a comparison of the bending stiffness and compressive stiffness is done. Since initially pressing the adhesive system on the curved substrate is a kind of bending test, the adhesive systems with the most contact area during preloading the adhesive system on the substrate, also have the lowest bending stiffness. These two stiffnesses are later compared as a check.

3.1.3 Contact area

Imaging of the contact area is done by the 'Frustrated total internal reflection' method (FTIR) [26, 51]. A white LED strip (micro 4x2 mm LED STRIP 69 leds/meter 5,5 W/meter 12 V Cold white 6000K. 628 lumen/m) is attached with duct-tape to and shines into the side of the curved glass substrate, see fig.15B. Much of the light is totally reflected within the glass (due to the curvature of the glass the incident angle for some of the light beams becomes to great after reflecting and the light escapes). When a medium with a refraction index higher than glass touches the glass, the light is scattered and effectively acts as a light source which a camera can capture, see figure 15A. The camera (smartphone Nokia

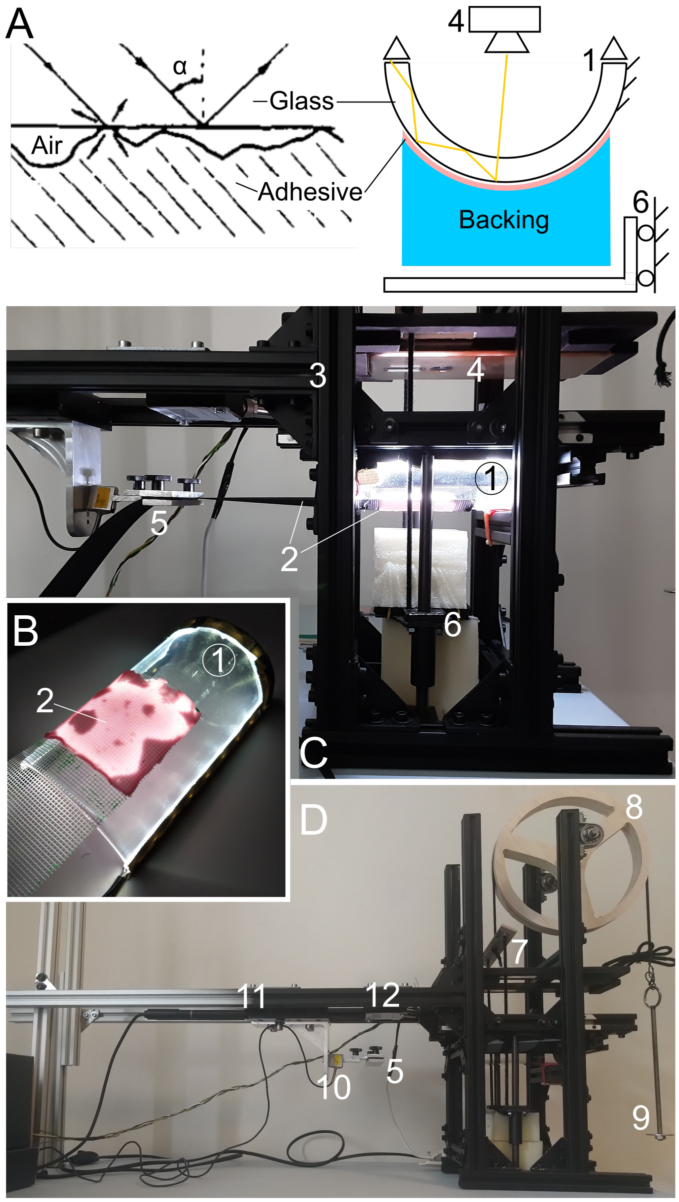

Fig. 15: Experimental setup to measure contact area and frictional load capacity. A: Left, schematic of Frustrated total internal reflection method, adapted from [47]. Right, schematic of FTIR in setup. B: The (glass) curved substrate with the light source (LED-strip) attached around the edges (1), and a (pilot) adhesive (2) on the convex side of the substrate. The areas where the adhesive makes contact with the glass are illuminated due to the internally reflecting light from the LED'S through the glass being scattered at those areas. C: The substrate from subfigure 'B' is mounted in a frame (3). The substrates concave side faces upwards to a camera (4). The tail of the adhesive (2) is clamped between two flat plates (5). An adhesive systems is brought into contact with the substrate by placing it on a platform (6), which slides vertically on two rods. D: The sliding platform is connected with two cables to a whiffle tree (7), which is connected to a pulley (8). On the other side of the pulley a weight (9) causes displacement of the platform and thereby creates a preload on an adhesive system. The clamp (5) is connected via a force sensor (10) to a linear actuator (11). A laser distance sensor (12) measures the displacement of the actuator.

7.1. setting: Daylight ISO100 1/500 shutter, 1000 pixels per mm^2) is placed some distance from the contact surface of the substrate, see fig. 15A&C. The image of the curved substrate is a distorted image of the contact plane and is therefore mapped to a flat plane with the Matlab functions: 'fitgeotrans' (option: 'lwm','12') and 'cpselect' (with 100 control points)(see apx.B fig.27). The control points, identifying the same spots of the distorted image in a flat plane, were made by laying a paper with $5\,\mathrm{mm} \times 5\,\mathrm{mm}$ grid on the curved substrate and on a flat plane (apx.B fig.28A-D).

For image analysis, a median filter (3 by 3 pixels) was used to remove dust spots but also removes some smaller contact points (apx.B fig.28G). Then, the image was converted to greyscale and binarised using Otsu's method (apx.B fig.28G). Pixels that are white indicate contact points and can be counted and converted to area.

3.1.4 Load capacity

The load capacity is measured with a force transducer (Futek miniature S-beam load sensor, LSB200 111 Newton version) in series with an electrical signal amplifier (Scaime CPJ Rail (Analog transmitter), which sends the signal to an A/D-converter connected to a computer (National Instruments USB-6008, analog to digital (A/D) converter, 8 inputs, 12-bit, 10 kS/s Multifunction I/O). The force transducer is attached to a linear actuator (Thorlabs Z825B) which is controlled by a motor controller (Thorlabs KDC101). The displacement of the actuator is measured with a distance sensor (Feteris optoNCDT1300, ILD 1300-50(000), 0904042, laser displacement sensor 50mm) connected to the same A/D converter. The sample rate of load and distance was both 100 ms.

The system is loaded parallel to the height direction of the cylindrical substrate. The adhesive's tail, is clamped $13\,\mathrm{cm}$ from the backing between two metal plates covered with double sided tape (GrippTek)(see apx.B fig.26). Since the clamp is flat and the substrate is cylindrical, the load angle varies with the radial position along the cylindrical substrate. If the adhesive system would make full contact, the outer edges would be loaded at $0°$ and to the center the load angle goes down to less than $0°$. At these angles, the friction force (which is the resisting force parallel to the substrate) due to adhesion, resists the actuator movement. Although the load angle is not always zero, the force sensor only picks up loads in one direction, the direction of parallel to the substrate, which is thus the friction load on the adhesive surface. The clamping distance of the tail is a compromise between the magnitude of variation of the load angle along the tail's width and the weight of the tail peeling on the edge of the adhesive system. The bolt connecting the clamp to the force sensor acts as a hinge which allows the clamp to rotate in the plane of the tail. This rotational freedom helps aligning the tail in the direction of the load path. The load path is fixed, the actuator displaces $9\,\mathrm{mm}$ at a velocity of $0.1\,\mathrm{mm\,s^{-1}}$.

Loading the adhesive system with the specified load path gives a load capacity versus distance curve for each specimen. The start of this curve is plotted when the load has reached $0.2\,\mathrm{N}$, which is four times the resolution of the force sensor. The distance samples are filtered with a moving

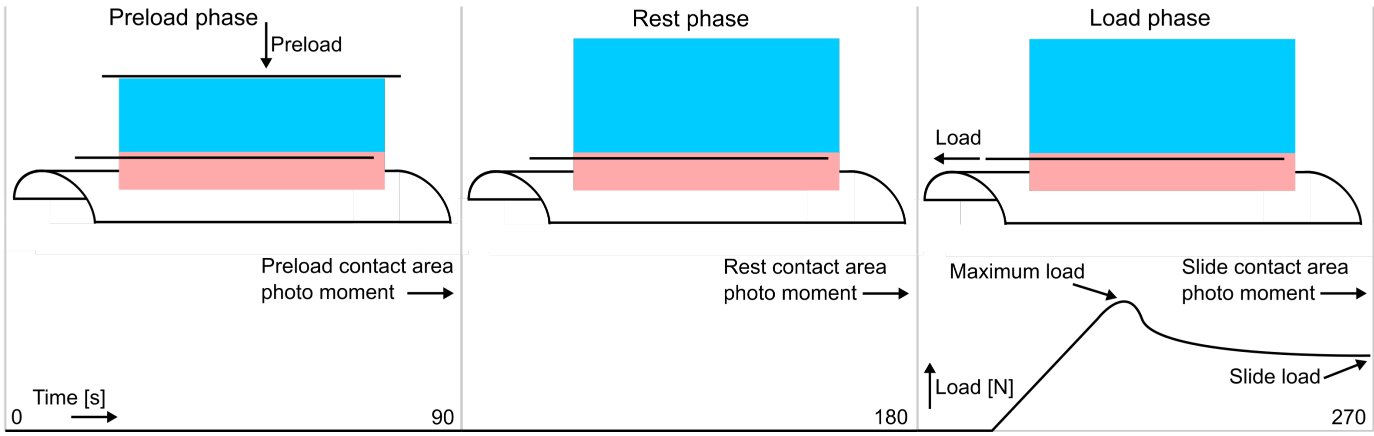

Fig. 16: Schematic of the test routine

mean filter of window size 10. The last $0.1\,\mathrm{mm}$ of the load distance curve is omitted due to sensor artifacts.

3.1.5 Preload

To preload an adhesive system, the adhesive system is placed onto a sliding platform and its tail clamped into the clamp (see fig.15C). The sliding platform is unbalanced by a counterweight giving a resultant force onto the adhesive system, pressing it onto the substrate, see fig.15D. The platform slides on two rods normal to the cylinders height. In a pilot study it was investigated in steps of $50\,\mathrm{g}$ at which preload the expected softest adhesive system variation would make full contact with the substrate. The normal preload for the PUR-sponge$_\mathrm{S}$ is: (3.61, 0.01)(mean [N], 3 standard deviations relative to the mean) and realised with a $500\,\mathrm{g}$ counterweight mass. This preload is also used for Rigid$_\mathrm{S}$. For the Inflatable$_\mathrm{S}$ a preload force was used for which the softest Inflatable did not fully 'collapse' (at which the sliding platform would almost touch the glass): (1.66, 0.01)(mean [N], 3 standard deviations relative to the mean) realised with a $300\,\mathrm{g}$ counterweight.

3.1.6 Test routine

A test is as follows (schematic in fig. 16): Before each test the substrate was cleaned with Isopropylalcohol on a paper wipe and then dried off with a paper wipe. The adhesive system is preloaded for $90\,\mathrm{s}$ called the 'preload phase', a photo of the contact area is made, the preload is removed for another $90\,\mathrm{s}$ called the 'rest phase', a photo is made, the system is loaded (actuator moves $9\,\mathrm{mm}$ in $90\,\mathrm{s}$) called the 'load phase', and finally a photo is made just before the actuator stops. The $90\,\mathrm{s}$ intervals are there to account for, in a pilot study observed, temporal decrease of the contact area. Contact area at the end of the preload phase is called the 'preload contact area'. Contact area at the end of the rest phase is called the 'rest contact area'. Contact area at the end of the load phase is called the 'slide contact area'. It is expected that an adhesive system is stuck on the substrate until the load reaches a maximum at which the system starts sliding over the substrate under a lower load. This maximum load will be called the 'maximum load'. The load at the end of the load measurement is called the 'slide load'.

3.1.7 Test order

The first of the two studies, used the adhesive systems PUR-sponge$_\mathrm{S}$ and Rigid$_\mathrm{S}$. Results of their frictional performance is compared between their variation specimens. The Rigid$_\mathrm{S}$ variations are use as control groups. For each backing variation there are 5 specimens and each specimen is tested 3 times. The order of the test was made up with the following sequence; A random choice of 15 possibilities out of all possibilities the 5 backing variations can be sequenced in (120 (factor 5)). These 15 random sequences are placed in successive order. Finishing first the first test for all 5 specimens of all backing variations before continuing with the second test, etc.

The second study used the Inflatable$_\mathrm{S}$. All Inflatable$_\mathrm{S}$ softness variations used the same specimen. Results of their frictional performance is compared between softness variations. Each variations was tested 5 times. The test order is based on successive rows of a balanced 6 by 6 Latin square [54] (each row contains each condition once, and for the whole square of rows applies that each condition is preceded by each other condition once), and omitting the last row.

3.1.8 Data analysis

Tukey's HSD Test for multiple comparisons, with a 95% confidence interval, on the mean value of the contact area in each phase, was done between all PUR-sponge$_\mathrm{S}$ variations and Rigid$_\mathrm{S}$ variations, and between all Inflatables$_\mathrm{S}$ variations.

A one-way ANOVA test was done to check whether there is a statistically significant difference in mean contact area between at least two variations of the PUR-sponge$_\mathrm{S}$ or Rigid$_\mathrm{S}$ in all phases, and between at least two variations of the Inflatable$_\mathrm{S}$.

From the preload, rest, and load phase photos, the respectively preload, rest, and slide contact areas are calculated. Since the maximum load capacity is expected to occur close to the rest contact area photo moment, a linear regression is done and a correlation coefficient calculated between these latter two. Since the slide load capacity is measured at the moment of the slide contact area, a linear regression is done and a correlation coefficient calculated between these latter two.

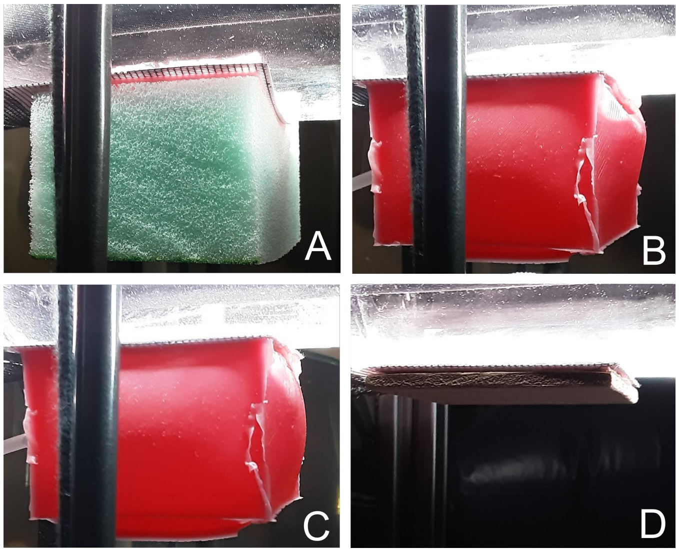

Fig. 17: Side view the adhesive systems types at different contact areas with the substrate. The contact areas correspond approximately (within $1\,\mathrm{cm}^2$) to the maximum measured contact area values in the experiment. A: $\mathrm{P_S}$-S, $23.5\,\mathrm{cm}^2$. B: $\mathrm{I_S}$-O1, $17\,\mathrm{cm}^2$. C: $\mathrm{I_S}$-C3, $10\,\mathrm{cm}^2$ ($10\,\mathrm{cm}^2$ is approximately the maximum contact area $\mathrm{I_S}$-C1 made in the experiment). D: $\mathrm{R_S}$-F, $4\,\mathrm{cm}^2$.

3.2 Experimental results

In general, systems with a softer backing made and kept the same or more contact area, and load capacity scaled positively with contact area.

For the side view of the adhesive systems at different contact area's see figure 17. Example photos of the contact areas at the different test phases are shown in appendix B figure 30.

Loading the adhesive system with the specified load path gave a load capacity versus distance curve for each specimen (see, apx.B fig.29). The trend of such a curve is as follows: an increase in load with increasing distance up to a maximum, then a decrease in load, and lastly a slightly decreasing load (plateau).

3.2.1 PUR-sponge system and Rigid system

Systems with the PUR-sponge backing made in all phases more contact than the ones with a rigid backing. In the preload phase, contact area scaled positively with sponge softness, and $\mathrm{R_S}$-C made in all phases more contact than $\mathrm{R_S}$-F. Significant difference between the contact area of $\mathrm{P_S}$-M and $\mathrm{P_S}$-H disappears in the rest and load phases. A one-way ANOVA revealed that there was a statistically significant difference in mean contact area between at least two variations of the PUR-sponges$_\mathrm{S}$ or Rigid$_\mathrm{S}$ in all phases (preload phase (F(4, 70) = 1106, p = 1.9e-62), rest phase (F(4, 70) = 403, p = 1.6e-47), load phase (F(4, 70) = 118, p = 2.0e-30)).

Load capacity scaled positively with contact area, in both the rest and load phases. In fact, for the PUR-sponge system, a linear regression analysis in the rest phase gives a relation between maximum load capacity M_P and the rest contact area A_r of $M_\mathrm{P} = 0.3\,\mathrm{N} + 2.2\,\mathrm{N\,cm^{-2}} \cdot A_\mathrm{r}$. A linear regression in load phase for PUR-sponges$_\mathrm{S}$ gives a relation between slide load capacity S_P and the slide contact area A_s of $S_\mathrm{P} = -1.9\,\mathrm{N} + 1.5\,\mathrm{N\,cm^{-2}} \cdot A_\mathrm{s}$. For the Rigid system, a linear regression analysis in the rest phase gives a relation between maximum load capacity M_R and the rest contact area A_r of $M_\mathrm{R} = 2.0\,\mathrm{N} + 1.8\,\mathrm{N\,cm^{-2}} \cdot A_\mathrm{r}$. A linear regression in load phase for Rigid$_\mathrm{S}$ gives a relation between slide load capacity S_R and the slide contact area A_s of $S_\mathrm{R} = 0.2\,\mathrm{N} + 1.2\,\mathrm{N\,cm^{-2}} \cdot A_\mathrm{s}$. Combining the data of PUR-sponge$_\mathrm{S}$ and Rigid$_\mathrm{S}$ gives a correlation coefficient between contact area and load capacity in the rest phase of 0.96, and in the load phase of 0.99.

Two specimens were removed from the data since one $\mathrm{P_S}$-H specimen showed stick-slip behavior, and one $\mathrm{R_S}$-C specimen fell (see apx.B fig.29B).

3.2.2 Inflatable system

An open Inflatable compared to a closed Inflatable with equal initial pressure, made more contact in all phases. For both a closed and open Inflatable, lower initial pressure results into more contact area in the preload and rest phases. In the load phase this difference is lost between $\mathrm{I_S}$-C1 and $\mathrm{I_S}$-C2, and between $\mathrm{I_S}$-O1 and $\mathrm{I_S}$-O2. A one-way ANOVA revealed that there was a statistically significant difference in mean contact area between at least two variations of the Inflatables$_\mathrm{S}$ (preload phase (F(5, 24) = 523, p = 1.1e-23), rest phase (F(5, 24) = 169, p = 6.6e-18), load phase (F(5, 24) = 24, p = 1.3e-08)).

Load capacity scaled positively with contact area, in both the rest and load phases. In fact, linear regression analysis in rest phase gives a relation between maximum load capacity M_I and the rest contact area A_r of $M_\mathrm{I} = 2.3\,\mathrm{N} + 1.6\,\mathrm{N\,cm^{-2}} \cdot A_\mathrm{r}$. The correlation coefficient between these is 0.96. A linear regression in load phase gives a relation between slide load capacity S_I and the slide contact area A_s of $S_\mathrm{I} = -0.1\,\mathrm{N} + 1.3\,\mathrm{N\,cm^{-2}} \cdot A_\mathrm{s}$. The correlation coefficient between these is 0.99.

3.3 Discussion experiment

3.3.1 Results

The contact areas in the preload phase agree with hypothesis 1 (a greater contact area is made with a softer backing) but the areas in the rest and load phases do not fully agree with hypothesis 2 (more contact is kept with a softer backing). This is likely due to time-dependent behavior of the systems and not their softness as will be discussed. The found positive correlations between contact area and load capacity (≥ 0.96), for a specific adhesive system type, underpins that more contact area results in a greater frictional load capacity, which was hypothesized. The lower correlation coefficient in rest phase (0.96) than in the load phase (0.99), is likely due to the higher relative variability ($r = 0.21$) of the maximum load (M_Av) of the adhesive compared to the slide load (S_Av) variability ($r = 0.07$)('r' is two standard deviations from the mean to the mean).

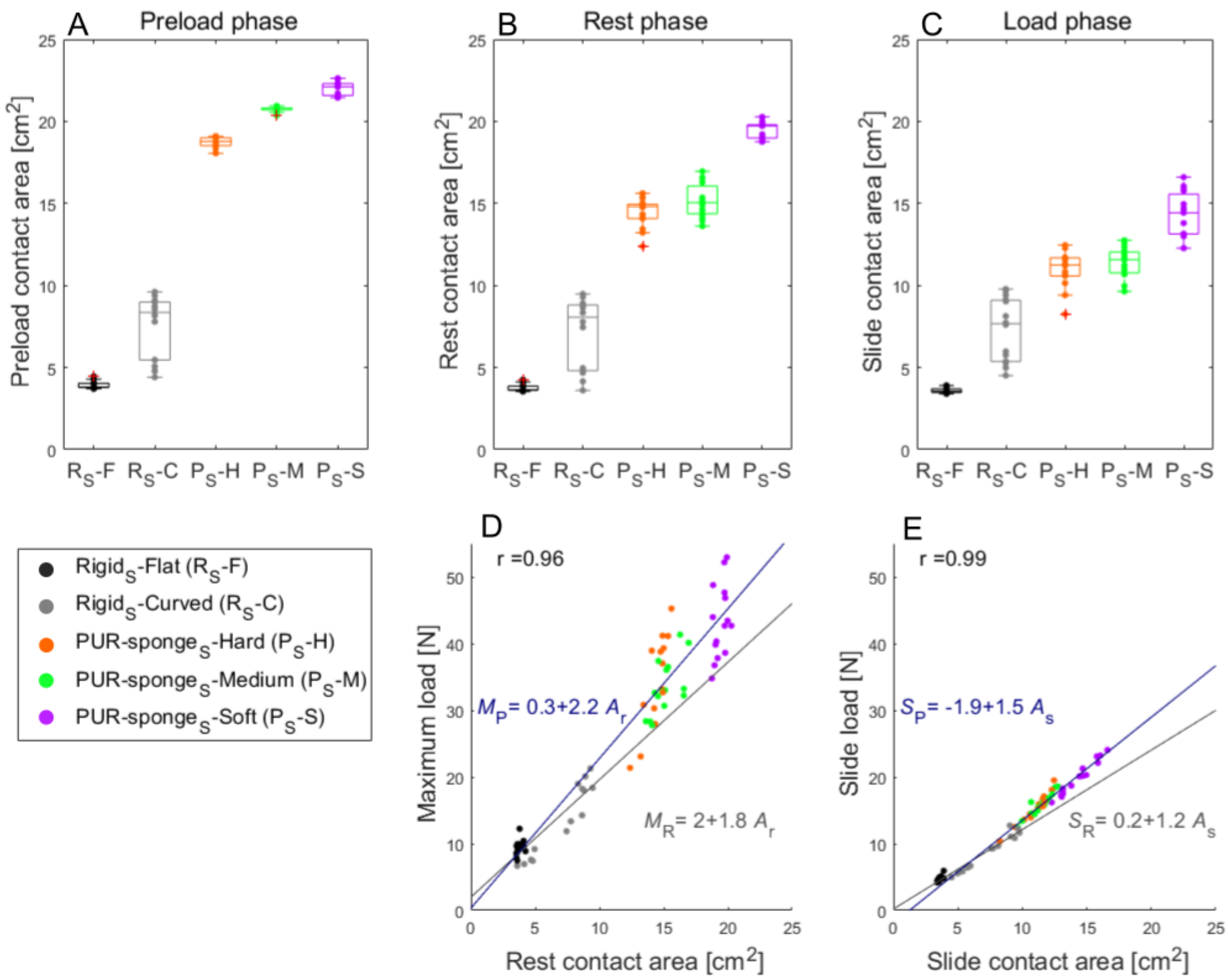

Fig. 18: Contact area and load capacity of the PUR-sponges$_S$ and Rigid$_S$ variations. A: Preload contact area B: Rest contact area C: Slide contact area. D: Rest contact area vs. maximum load capacity E: Slide contact area vs. slide load capacity.

3.3.1.1 PUR-sponge system:

The PUR-sponge system variation with a softer backing made, as hypothesized, more contact with the substrate under the constant preload. As opposed to the second hypothesis, a softer backing did not always result in keeping more contact. This was due to the lack of a significant difference in contact area between P$_S$-M and P$_S$-H in the rest and load phases. This might be explained by the time dependent behavior of the PUR-sponges. Whereas the stress-strain curve of P-M is lower than the one of P-H when compressed, they are close to each other on the return stroke (fig.11D). The compression moduli at 17% compression, of P-M and P-H on the return stroke are $4.7\,\mathrm{kPa}$ and $4.8\,\mathrm{kPa}$ respectively, while they were $8\,\mathrm{kPa}$ and $10.5\,\mathrm{kPa}$ on the compression stroke (fig.22). This means that P-H is more viscous. The viscosity delays the elastic spring-back of the sponge which means less of the internal stresses have to be balanced by the adhesion forces. An extra experiment was done to investigate this time dependent behavior, referred to as 'experiment$_T$'. Three specimens of each PUR-sponge system variation (P$_S$-S, P$_S$-M, and P$_S$-H) were pressed onto the substrate until full contact was made. After removing this preload the adhesive systems peeled off the substrate in time due to the internal stresses being unbalanced with adhesive forces. The contact area was measured in time (apx.B fig.31). The results of experiment$_T$ suggest that P$_S$-M and P$_S$-H peeled off the substrate at the same rate (loss of contact area with time). Indicating that their compression moduli are similar after compression (when they try to return to their original shape). Although having a similar rate would make this time dependency seemingly unimportant when it is about differences between two systems, the rate decreases with time. This means that the contact area difference decreases with time as well. Therefore, it is likely that the insignificant results in contact area between P$_S$-M and P$_S$-H in the experiment are due to their similar softness after compression. Thereby these results would not oppose the second hypothesis.

3.3.1.2 Inflatable system:

The Inflatable system with a softer backing made, as hypothesized, more contact with the substrate under the constant preload. As opposed to the second hypothesis, a softer backing did not always result in keeping more contact. This is because the difference between I$_S$-O1 and I$_S$-O2, and between I$_S$-C1 and I$_S$-C2 became insignificant in the load phase. Which might again be explained by the decreasing rate of loss of contact area, which makes differences

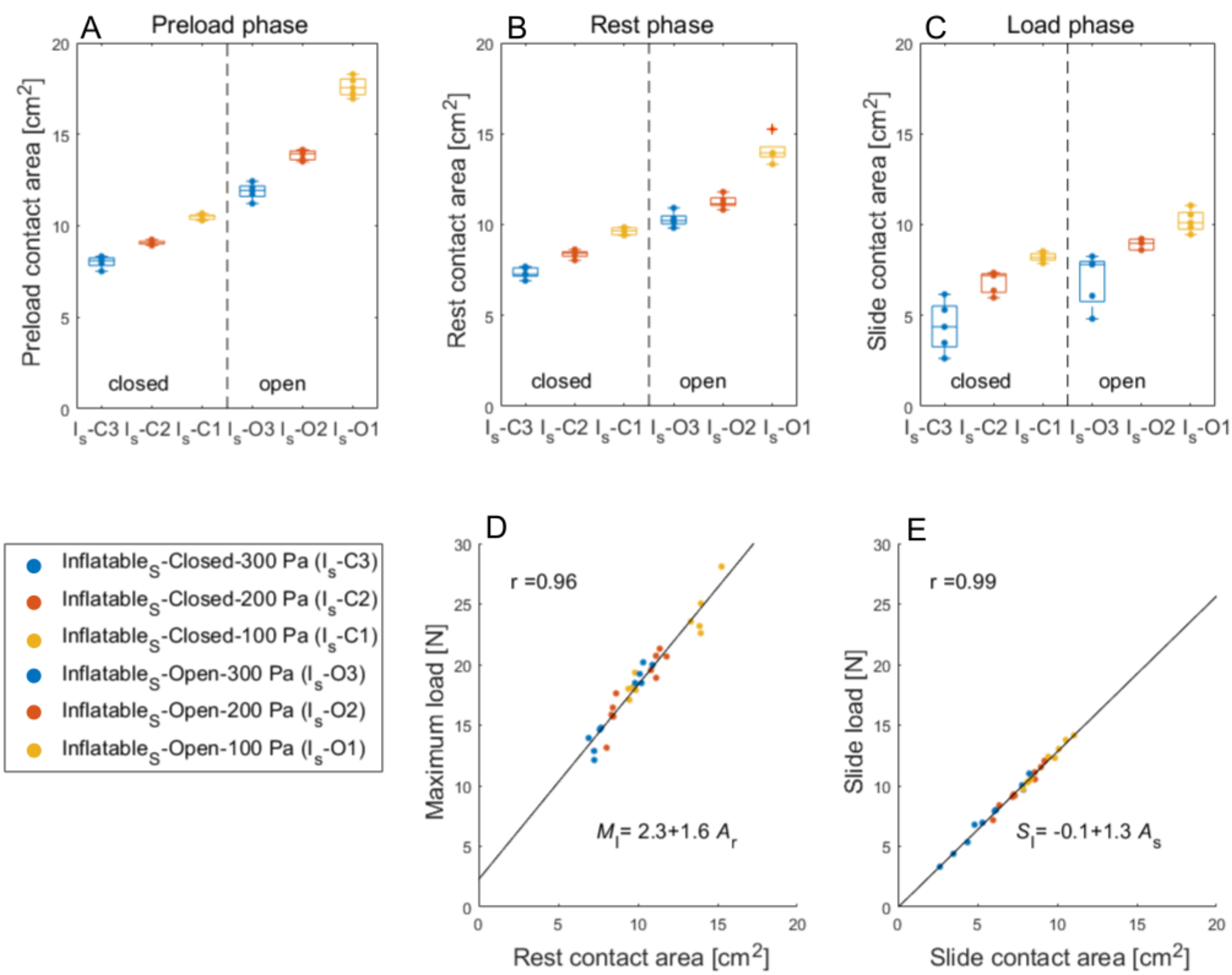

Fig. 19: Contact area and load capacity of the Inflatables$_S$ variations. A: Preload contact area B: Rest contact area C: Slide contact area. D: Rest contact area vs. maximum load capacity E: Slide contact area vs. slide load capacity.

between systems smaller. This is under the assumption that the 'contact area in time' curves will overlap with time for these systems. Figure 32A,B (apx.B) seem to indicate that the curves of I_S-O1 and I_S-O2 overlap more than with I_S-O3, and I_S-C1 and I_S-C2 overlap more than with I_S-C3. Which could explain why these lose significant difference in contact area in the load phase.

In experiment$_T$ with the Inflatables$_S$ (apx.B fig.32)C-E, it is seen that for a variation with a certain initial pressure, the contact area drops faster for the closed variation, compared to the open variation, but after some time ($\approx$ 3 min) the rate of contact area loss and contact area magnitude are similar to that of the open variation. This is likely due to the Inflatable being almost in the same state when contact area is low, since at that moment the inflatable is barely deformed. Still, in the experiment, differences in contact area stayed great enough in time to be significant in all phases between an open and closed variation with the same initial pressure.

3.3.2 Method

The compressive stiffness of the backings was quantified by measuring their stress-strain curves. Pressing the adhesive system on the curved substrate acts as a bending test, this happened in the preload phase in the experiment. Comparing the contact area's of the systems in the preload phase (fig.18A & fig.19A) with the compression moduli of the respectively backings (fig.22), it follows that backings with a lower compression modulus made more contact with the substrate. This indicates that the compression stiffness was a valid proxy for softness of the backings.

In experiment$_T$ it was seen that the rate of loss of contact area decreases with time. Thus, using a time interval of $90\,\mathrm{s}$, instead of no time interval, for the rest phase, made the difference smaller between the rest contact area and the contact area at the moment the maximum load occurs. Still, contact area decreases with time after $90\,\mathrm{s}$ and therefore the maximum load capacities as function of the rest contact area, are an underestimation of the maximum load as function of the contact area at the moment of maximum load. Strangely, even without taking this underestimation into account, the tenacity of adhesive is lower than that of the PUR-sponges$_S$, in both the rest phase ($2.1\,\mathrm{N/cm^2}$ vs. $2.2\,\mathrm{N/cm^2}$) and load phase ($1.3\,\mathrm{N/cm^2}$ vs. $1.5\,\mathrm{N/cm^2}$). It was expected that the tenacity of the adhesive would be higher since it has no backing introducing extra stress on it. Although the results indicate a linear relation between contact area and load capacity, it could be that this relation is lost at the highest contact area of the adhesive ($25\,\mathrm{cm^2}$) that was used to calculate the tenacity of the adhesive, and that this increased contact area negatively impacted the tenacity. The difference could also be due to the difference in time between the measurements for adhesive characterization and frictional load capacity, which was a couple weeks. In this time the adhesive material could have changed since it did not used the standard 20/20 parts 'a' to 'b' ratio.

Since the slide contact area is at a different location on the substrate than the rest and preload contact areas (apx.B fig.30), the load plateau, seen in the load versus distance curves, overlaps with the adhesive system sliding over the substrate. The load at this plateau is likely lower than the maximum load since dynamic friction is lower than static friction.

4 Conclusion

This section starts with conclusions drawn from the experiment and the backing design. Then, some insights in the biological backings, that were used as inspiration for backing design concepts, are stated. The conclusion ends with the implications of this study on synthetic dry adhesive systems.

Taking time-dependent effects of the systems into account, the experiment results are in agreement with the hypotheses stated in the introduction. This implies that a dry adhesive system will benefit from a softer backing by making and keeping more contact with a substrate and consequentially has a higher load capacity.

In the experiment it was also seen that the rigid system did not make full contact on neither the curved or flat substrate. This Underlines the need for a soft backing. The backing design concepts, inflatable and sponge, proved to be a softer backing design than the solid concept when made with the same material, as shown with the silicone specimens. Another advantage of the inflatable concept was expected to be that the internal fluid helps distribute contact stress more evenly since the pressure in the fluid is everywhere even. However, only the sponge concept distributed the preload relatively even at low and high compression, owing it to its stress plateau in its compression stress-strain characteristic, giving it a similar stress in the material for a range of deformations. Although the open Inflatable has an equal pressure internally and also shows such a plateau, it was found that its contact stress is not even, due to the presence of its outer hull. Inflatable grippers with a negative pressure also show an effect of the hull on the resulting contact stress [**?**]. The internal overpressure will only change the initial hull shape and increases stiffness of the inflatable [26]. Thus now the case is made that internal fluid, which is always contained by some outer hull, is often more of a hindrance compared to the empty hull. More importantly than the preload stress distribution, would be the distribution after removal of the preload. A more even contact stress distribution, when the preload is removed, would help reduce stress concentrations that might peel the adhesive system from the substrate. Materials with a plateau in their tensile stress-strain relation could give a stress distribution with reduced contact stress concentrations. Such measurement, other materials, and new backing concepts can be future work.

4.1 Insights in biological backings

Here, 4 insights are stated in regard to the biological backing softness, structure and shape.

The experiment results indicate functional relevance of the presence of a relatively large and soft volume between the most distal toe/finger phalanx and the adhesive surface in geckos, tree frogs and humans. Furthermore, the inflatable concept in its open variations, was softer than its closed variations. This suggests functional relevance of the fluids found in the biological systems being part of their circulatory system (known for the gecko and human).

Although both the more adhesive oriented gecko and tree frog system have a large fluid filled region in this soft backing volume, and the less adhesive oriented human system has not, it is unclear whether this indicates relevance of the inflatable backing concept instead of the open celled sponge concept. It might be the case that the inflatable is the result of a sponge 'design' in the bio-system, in which larger cells became more useful. It could be that these cells happened to fill up with fluid and are closed off by the dermis, since it is an organism, making it look like an inflatable.

The shape of the adhesive systems used were cuboid and their adhesive surface therefore planar, in contrast to the bio-adhesive surfaces which are convex (tree frog [55]). Gu et al. suggested that the ball-on-flat arrangement of a curved pad on a flat substrate protects a tree frog's pad from misalignment [56]. Langowski et al. suggested that, a curved tree frog toe pad might require less energy for active alignment of the pad with respect to the substrate [6]. Another benefit of a convex finger/toe pad surface could be the following. Contact between a planar adhesive and concave substrate is difficult since the adhesive makes first contact with the higher region of the substrate and has, if stuck there, to be stretched to come into further contact with the lower center area. This extra stretching likely introduces more internal stresses than the required bending of the adhesive would for an one-dimensional concave substrate. A convex shape of the adhesive surface could allow the adhesive system to make contact in the lower center region of a concave substrate first, increasing the range of suitable curvatures to attach to.

4.2 Implications on synthetic dry adhesive systems

It is expected that the found increased frictional performance with increased backing softness of the tested adhesive systems, translates to other systems with different types of backings. Not only on a cylindrical substrate but to other substrate shapes as well, as the story of lower internal stresses with softer backings will be similar.

Different backing types can be made with different structures, materials, and outer shapes. Also, when the reinforcement is not parallel to the adhesive surface, the reinforcement is bound to pass through the backing. The backing, adhesive material and reinforcement can be made together as a composite [57], although the availability of soft materials in composite manufacturing are still rare.

Soft backings could already be added to existing grippers that use a similar adhesive as in this study. This includes grippers made from a stiff material [25, 17]. But also to soft pneumatic grippers [28]. With increased internal pressure in such grippers the grip force increases but the gripper becomes stiffer as well, which negatively impacts contact area [26]. As example of a soft backing addition to these existing grippers, the soft pneumatic gripper with a PUR-sponge layer as gripping surface of Galloway et al. can be looked at [27]. Furthermore, open celled sponge backings might be useful inside a negative internal pressure gripper [58] to distribute the preload.

Concluding, the addition of a soft backing to help make and keep more contact with a substrate, and thereby increasing load capacity, promises a new design paradigm in synthetic dry adhesives.

Acknowledgment

The author thanks Dimitra Dodou and Julian Langowski for their guidance.

References

[1] Y. Han, H. Marvi, and M. Sitti, "Fiberbot: A miniature crawling robot using a directional fibrillar pad," *Proceedings - IEEE International Conference on Robotics and Automation*, vol. 2015-June, no. June, pp. 3122–3127, 2015.

[2] H. Chen, L. Zhang, D. Zhang, P. Zhang, and Z. Han, "Bioinspired Surface for Surgical Graspers Based on the Strong Wet Friction of Tree Frog Toe Pads," *ACS Applied Materials and Interfaces*, vol. 7, no. 25, pp. 13 987–13 995, 2015.

[3] H. Jiang, E. W. Hawkes, C. Fuller, M. A. Estrada, S. A. Suresh, N. Abcouwer, A. K. Han, S. Wang, C. J. Ploch, A. Parness, and M. R. Cutkosky, "A robotic device using gecko-inspired adhesives can grasp and manipulate large objects in microgravity," *Science Robotics*, vol. 2, no. 7, pp. 1–12, 2017.

[4] E. W. Hawkes, E. V. Eason, D. L. Christensen, and M. R. Cutkosky, "Human climbing with efficiently scaled gecko-inspired dry adhesives," *Journal of the Royal Society Interface*, vol. 12, no. 102, 2015.

[5] A. P. Russell, A. Y. Stark, and T. E. Higham, "The Integrative Biology of Gecko Adhesion: Historical Review, Current Understanding, and Grand Challenges," *Integrative and Comparative Biology*, vol. 59, no. 1, pp. 101–116, 2019.

[6] J. K. Langowski, D. Dodou, M. Kamperman, and J. L. van Leeuwen, "Tree frog attachment: Mechanisms, challenges, and perspectives," *Frontiers in Zoology*, vol. 15, no. 1, 2018.

[7] M. D. Bartlett, A. B. Croll, D. R. King, B. M. Paret, D. J. Irschick, and A. J. Crosby, "Looking beyond fibrillar features to scale gecko-like adhesion," *Advanced Materials*, vol. 24, no. 8, pp. 1078–1083, 2012.

[8] K. Kendall, "Thin-film peeling-the elastic term," *Journal of Physics D: Applied Physics*, vol. 8, no. 13, pp. 1449–1452, 1975.

[9] S. Ponce, J. Bico, and B. Roman, "Effect of friction on the peeling test at zero-degrees," *Soft Matter*, vol. 11, no. 48, pp. 9281–9290, 2015.

[10] D. R. King and A. J. Crosby, "Optimizing Adhesive Design by Understanding Compliance," *ACS Applied Materials and Interfaces*, vol. 7, no. 50, pp. 27 771–27 781, 2015.

[11] S. Abbot, "Dahlquist Criterion." [Online]. Available: https://www.stevenabbott.co.uk/practical-adhesion/dahlquist.php

[12] L. Xue, A. Luo, K. T. Turner, X. Wang, D. Tan, R. Zhang, H. Du, M. Steinhart, C. Mijangos, M. Guttmann, M. Kappl, B. Sanz, A. Luo, K. T. Turner, X. Wang, D. Tan, R. Zhang, H. Du, M. Steinhart, C. Mijangos, M. Guttmann, M. Kappl, A. Del Campo, B. Sanz, A. Luo, K. T. Turner, X. Wang, D. Tan, R. Zhang, H. Du, M. Steinhart, C. Mijangos, M. Guttmann, M. Kappl, and A. Del Campo, "Hybrid Surface Patterns Mimicking the Design," *ACS Nano*, vol. 11, no. 10, pp. 9711–9719, oct 2017.

[13] Z. Wang, "Slanted Functional Gradient Micropillars for Optimal Bioinspired Dry Adhesion," *ACS Nano*, vol. 12, no. 2, pp. 1273–1284, 2018.

[14] X. Wang, D. Tan, X. Zhang, Y. Lei, and L. Xue, "Effective elastic modulus of structured adhesives: From biology to biomimetics," *Biomimetics*, vol. 2, no. 3, 2017.

[15] P. Birkmeyer, A. G. Gillies, and R. S. Fearing, "Dynamic climbing of near-vertical smooth surfaces," *IEEE International Conference on Intelligent Robots and Systems*, pp. 286–292, 2012.

[16] E. W. Hawkes, E. V. Eason, A. T. Asbeck, and M. R. Cutkosky, "The Gecko's toe: Scaling directional adhesives for climbing applications," *IEEE/ASME Transactions on Mechatronics*, vol. 18, no. 2, pp. 518–526, 2013.

[17] P. van Assenbergh, C. Culmone, P. Breedveld, and D. Dodou, "Implementation of anisotropic soft pads in a surgical gripper for secure and gentle grip on vulnerable tissues," *Proceedings of the Institution of Mechanical Engineers, Part H: Journal of Engineering in Medicine*, vol. 235, no. 3, pp. 255–263, 2021.

[18] E. Brown, N. Rodenberg, J. Amend, A. Mozeika, E. Steltz, M. R. Zakin, H. Lipson, and H. M. Jaeger, "Universal robotic gripper based on the jamming of granular material," *Proceedings of the National Academy of Sciences of the United States of America*, vol. 107, no. 44, pp. 18 809–18 814, 2010.

[19] J. Eisenhaure and S. Kim, "An Internally Heated Shape Memory Polymer Dry Adhesive," *Polymers*, vol. 6, no. 8, pp. 2274–2286, 2014.

[20] M. R. Cutkosky, "Climbing with adhesion: From bioinspiration to biounderstanding," *Interface Focus*, vol. 5, no. 4, 2015.

[21] S. Wang, H. Jiang, and M. R. Cutkosky, "Design and modeling of linearly-constrained compliant spines for human-scale locomotion on rocky surfaces," *International Journal of Robotics Research*, vol. 36, no. 9, pp. 985–999, 2017.

[22] H. Jiang, E. W. Hawkes, V. Arutyunov, J. Tims, C. Fuller, J. P. King, C. Seubert, H. L. Chang, A. Parness, and M. R. Cutkosky, "Scaling controllable adhesives to grapple floating objects in space," *Proceedings - IEEE International Conference on Robotics and Automation*, vol. 2015-June, no. June, pp. 2828–2835, 2015.

[23] W. Ruotolo, F. S. Roig, and M. R. Cutkosky, "Load-sharing in soft and spiny paws for a large climbing robot," *IEEE Robotics and Automation Letters*, vol. 4, no. 2, pp. 1439–1446, 2019.

[24] D. Ruffatto, D. Beganovic, A. Parness, and M. Spenko, "Experimental evaluation of adhesive technologies for robotic grippers on micro-rough surfaces," *2014 IEEE International Conference on Robotics and Automation (ICRA)*, pp. 6150–6155, 2014.

[25] M. J. D. Hullu, "Development of an adhesive grasper for Minimally Invasive Surgery," Ph.D. dissertation, TU Delft, 2011.

[26] P. Glick, S. A. Suresh, D. Ruffatto, M. Cutkosky, M. T. Tolley, and A. Parness, "A Soft Robotic Gripper with Gecko-Inspired Adhesive," *IEEE Robotics and Automation Letters*, vol. 3, no. 2, pp. 903–910, 2018.

[27] K. C. Galloway, K. P. Becker, B. Phillips, J. Kirby, S. Licht, D. Tchernov, R. J. Wood, and D. F. Gruber, "Soft Robotic Grippers for Biological Sampling on Deep Reefs," *Soft Robotics*, vol. 3, no. 1, pp. 23–33, 2016.

[28] P. Polygerinos, Z. Wang, K. C. Galloway, R. J. Wood, and C. J. Walsh, "Soft robotic glove for combined assistance and at-home rehabilitation," *Robotics and Autonomous Systems*, vol. 73, pp. 135–143, 2015. [Online]. Available: http://dx.doi.org/10.1016/j.robot.2014.08.014

[29] J. K. Langowski, H. Schipper, A. Blij, F. T. van den Berg, S. W. Gussekloo, and J. L. van Leeuwen, "Force-transmitting structures in the digital pads of the tree frog Hyla cinerea: a functional interpretation," *Journal of Anatomy*, vol. 233, no. 4, pp. 478–495, 2018.

[30] A. P. Russell, "Descriptive and Functional Anatomy of the Digital Vascular System of the Tokay , Gekko gecko," vol. 323, pp. 293–323, 1981.

[31] S. L. Peterson, E. L. Peterson, and M. J. Wheatley, "Management of fingertip amputations," *Journal of Hand Surgery*, vol. 39, no. 10, pp. 2093–2101, 2014. [Online]. Available: http://dx.doi.org/10.1016/j.jhsa.2014.04.025

[32] A. P. Russell, "The morphological basis of weight-bearing in the scansors of the tokay gecko (Reptilia: Sauria)," *Canadian Journal of Zoology*, vol. 64, no. 4, pp. 948–955, 1986.

[33] A. Ecker and R. Wiedersheim, *Anatomie des frosches*. FRIEDRICH VIEWEG UND SOHN, 1897.

[34] W. Federle, W. J. Barnes, W. Baumgartner, P. Drechsler, and J. M. Smith, "Wet but not slippery: Boundary friction in tree frog adhesive toe pads," *Journal of the Royal Society Interface*, vol. 3, no. 10, pp. 689–697, 2006.

[35] J. K. A. Langowski, S. Singla, A. Nyarko, H. Schipper, and F. T. V. D. Berg, "Comparative and functional analysis of the digital mucus glands and secretions of tree frogs Comparative and functional analysis of the digital mucus glands and secretions of tree frogs," 2019.

[36] K. Autumn, C. Majidi, R. E. Groff, A. Dittmore, and R. Fearing,

"Effective elastic modulus of isolated gecko setal arrays," *Journal of Experimental Biology*, vol. 209, no. 18, pp. 3558–3568, 2006.

[37] A. P. Russell and M. K. Johnson, "Real-world challenges to, and capabilities of, the gekkotan adhesive system: Contrasting the rough and the smooth," *Canadian Journal of Zoology*, vol. 85, no. 12, pp. 1228–1238, 2007.

[38] Y. Tian, J. Wan, N. Pesika, and M. Zhou, "Bridging nanocontacts to macroscale gecko adhesion by sliding soft lamellar skin supported setal array," *Scientific Reports*, vol. 3, pp. 1–6, 2013.

[39] S. Derler, L. C. Gerhardt, A. Lenz, E. Bertaux, and M. Hadad, "Friction of human skin against smooth and rough glass as a function of the contact pressure," *Tribology International*, vol. 42, no. 11-12, pp. 1565–1574, 2009. [Online]. Available: http://dx.doi.org/10.1016/j.triboint.2008.11.009

[40] M. J. Adams, B. J. Briscoe, and S. A. Johnson, "Friction and lubrication of human skin," *Tribology Letters*, vol. 26, no. 3, pp. 239–253, 2007.

[41] X. Liang, "Biomechanical Properties of In Vivo Human Skin From Dynamic Optical Coherence Elastography," *IEEE Trans Biomed Eng.*, vol. 57, no. 4, pp. 953–959, 2013.

[42] F. Hendriks, "Mechanical behaviour of human epidermal and dermal layers in vivo," Ph.D. dissertation, TU Eindhoven, 2005. [Online]. Available: http://en.scientificcommons.org/17601300

[43] R. F. Friesen, M. Wiertlewski, M. A. Peshkin, and J. E. Colgate, "Bioinspired artificial fingertips that exhibit friction reduction when subjected to transverse ultrasonic vibrations," *IEEE World Haptics Conference*, 2015.

[44] Y. Li, D. Zhu, S. Handschuh-Wang, G. Lv, J. Wang, T. Li, C. Chen, C. He, J. Zhang, Y. Liu, B. Yang, and X. Zhou, "Bioinspired, Mechano-Regulated Interfaces for Rationally Designed, Dynamically Controlled Collection of Oil Spills from Water," *Global Challenges*, vol. 1, no. 3, p. 1600014, 2017.

[45] K. J. , "Silicone Foam from Silicone Caulk." [Online]. Available: http://www.observationsblog.com/sciencetechnologyexperiments/silicone-foam-from-silicone-caulk#comments

[46] W. Yu, Y. Li, Y. P. Zheng, N. Y. Lim, M. H. Lu, and J. Fan, "Softness measurements for open-cell foam materials and human soft tissue," *Measurement Science and Technology*, vol. 17, no. 7, pp. 1785–1791, 2006.

[47] R. P. Betts, T. Duckworth, I. G. Austin, S. P. Crocker, and S. Moore, "Critical light reflection at a plastic/glass interface and its application to foot pressure measurements," *Journal of Medical Engineering and Technology*, vol. 4, no. 3, pp. 136–142, 1980.

[48] J. R. Barber, "Multiscale surfaces and Amontons' Law of Friction," *Tribology Letters*, vol. 49, no. 3, pp. 539–543, 2013.

[49] J. Archard, "Elastic deformation and the laws of friction," *Unknown*, no. 1, pp. 190–205, 1956.

[50] M. Wiertlewski, R. F. Friesen, and J. E. Colgate, "Partial squeeze film levitation modulates fingertip friction," *Proceedings of the National Academy of Sciences of the United States of America*, vol. 113, no. 33, pp. 9210–9215, 2016.

[51] I. D. Hill, B. Dong, W. J. P. Barnes, A. Ji, and T. Endlein, "The biomechanics of tree frogs climbing curved surfaces: a gripping problem," *The Journal of experimental biology*, vol. 221, 2018.

[52] S. Song, D. M. Drotlef, J. Paik, C. Majidi, and M. Sitti, "Mechanics of a pressure-controlled adhesive membrane for soft robotic gripping on curved surfaces," *Extreme Mechanics Letters*, vol. 30, p. 100485, 2019. [Online]. Available: https://doi.org/10.1016/j.eml.2019.100485

[53] E. V. Eason, E. W. Hawkes, M. Windheim, D. L. Christensen, T. Libby, and M. R. Cutkosky, "Stress distribution and contact area measurements of a gecko toe using a high-resolution tactile sensor," *Bioinspiration and Biomimetics*, vol. 10, no. 1, p. 16013, 2015. [Online]. Available: http://dx.doi.org/10.1088/1748-3190/10/1/016013

[54] E. J. Williams, "Experimental Designs Balanced for the Estimation of Residual Effects of Treatments," *Australian Journal of Chemistry*, vol. 2, no. 2, pp. 149–168, 1949.

[55] C. M. Richards, B. M. Carlson, T. G. Connelly, S. L. Rogers, and E. Ashcraft, "A scanning electron microscopic study of differentiation of the digital pad in regenerating digits of the kenyan reed frog, Hyperolius viridiflavus ferniquei." *Journal of morphology*, vol. 153, no. 3, pp. 387–395, sep 1977.

[56] Z. Gu, S. Li, F. Zhang, and S. Wang, "Understanding surface adhesion in nature: A peeling model," *Advanced Science*, vol. 3, no. 7, pp. 1–13, 2016.

[57] N. Glaser, "Decision making tool and review of fabrication methods for composite materials," TU Delft, Tech. Rep., 2021.

[58] S. Song, D.-m. Drotlef, C. Majidi, and M. Sitti, "Controllable load sharing for soft adhesive interfaces on three-dimensional surfaces," 2017.

APPENDIX A
DESIGN OF ADHESIVE SYSTEM EXTRAS

TABLE 2: Dimensions backing variations

Name	Height[1] (H)[mm]	Width[1] (W)[mm]	Length[1] [mm]	H/W	Force sensor (N version)	Remark
H-2	36.5 (0.5)	50	50	0.73	100	
H-3	38	50	50	0.76	100	
H-4	38	50	50	0.76	100	
S-4/20	18.35 (0.15)	29.55 (0.05)	29.6 (0.4)	0.62	100[2]	
S-20/20	18.6 (0.1)	29.3 (0.4)	29.45 (0.3)	0.63	10	
S-20/16	19.0	29.2 (0.2)	29.05 (0.15)	0.65	10	
S-20/14	34.6 (0.1)	50.85 (0.45)	50.2 (0.2)	0.7	100	
S-20/12	20.3	32.8	33.0	0.62	10	
S-20/10	16.25 (0.5)	31.3 (0.9)	32.0 (1.6)	0.52	100[2]	
Inflatable	35	50	50	0.7	10	
P-H	35 (1.0)	50 (1.0)	50 (1.0)	0.7	10	3 specimens, cut from ≈35 mm sheet
P-M	36 (1.0)	50 (1.0)	50 (1.0)	0.72	10	3 specimens, cut from ≈36 mm sheet
P-S	34 (1.0)	50 (1.0)	50 (1.0)	0.68	10	3 specimens, cut from ≈34 mm sheet
M-20/16	35.0	49.8	49.8	0.70	100	
M-20/15	22.0	33.5	33.5	0.66	10	
M-20/14	22.7	32.8	32.7	0.68	10	
M-20/13	21.05 (0.15)	32.3	32.5	0.65	10	
V-20/20	33.4	50.75	49.85	0.66	100	
V-20/16	33.05 (0.25)	33.8 (0.4)	33.2 (0.6)	0.98	10	
V-20/15	32.9 (0.3)	33.75 (0.25)	33.0	0.97	10	
V-20/14	31.95 (0.25)	32.8 (0.4)	32.95 (0.25)	0.97	10	
V-20/13	28.15 (1.15)	32.85 (1.45)	33.7 (0.5)	0.86	10	
F-1/2-1	27.0 (1.0)	29.5 (0.5)	30.0	0.92	100[3]	
F-1/2-2	33.0 (0.5)	37.7 (0.3)	36.0 (1.0)	0.87	100[3]	
F-1/2-3	27.75 (0.15)	40.8 (0.6)	39.55 (0.45)	0.68	10	
F-1/3.5	27.5 (0.5)	43.0 (2.0)	43.5 (0.5)	0.64	100[3]	
F-1/5	14.5	21.0	20.4	0.69	100[3]	

[1] Dimensions with a decimal place are measured with a 0.1 mm resolution caliper. Due to the roughness of the specimens a measurement of a side is taken at two places giving a minimum and maximum value. The value in brackets indicates the measured range, e.g. 10 (0.1) means 9.9-10.1.
[2] Force filter (moving mean, window size 15) used since the number of samples points were few due to the small dimensions.
[3] Force filter (moving mean, window size 15) used since measured forces were relatively small compared to the force resolution.

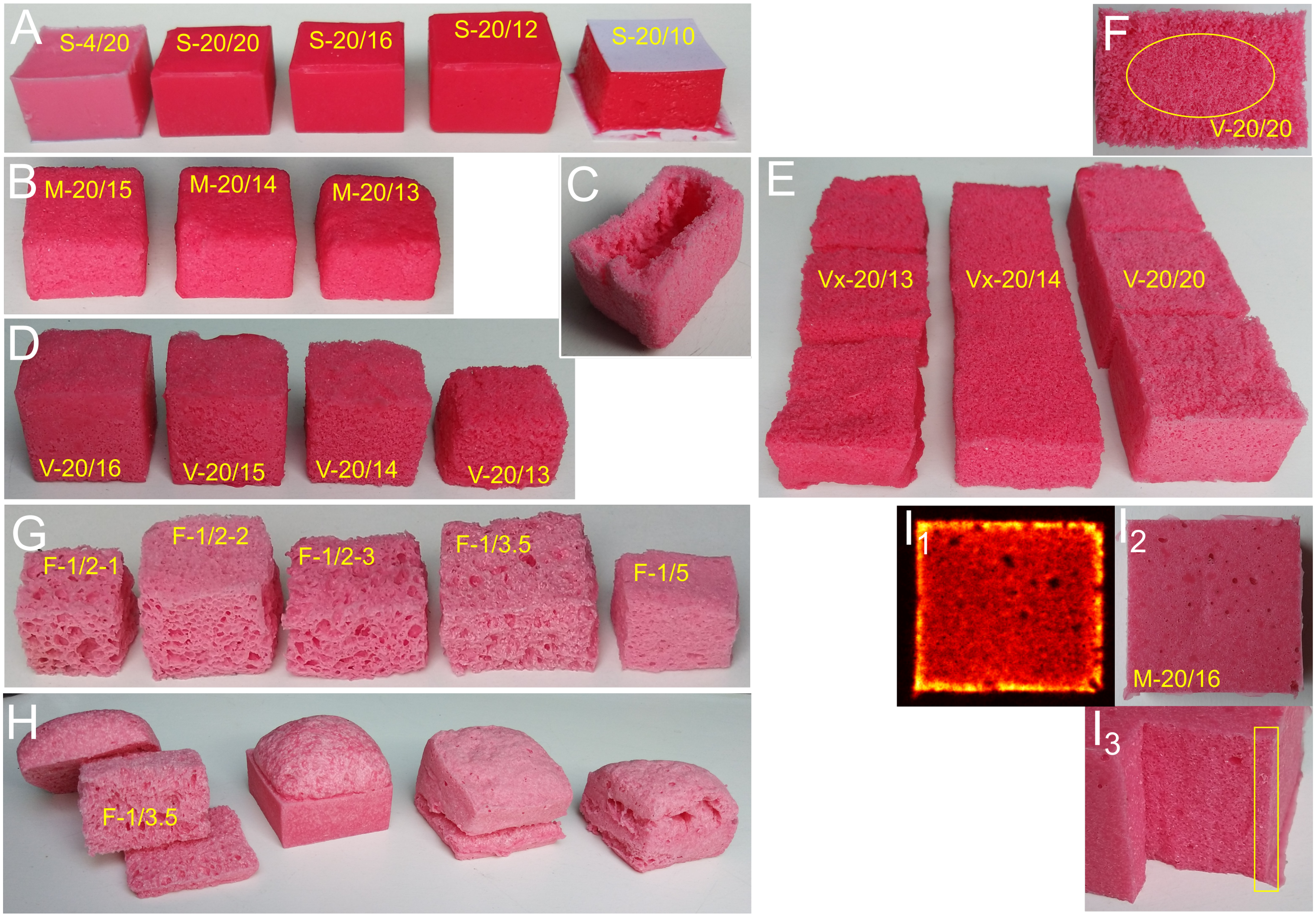

Fig. 20: Fabricated backing type variations not presented in the paper. variation names in yellow. A: Silicone variations. S-20/10 is fragile and has two paper sides for handling B: 'Sponge by mixing' variations. C: Half of a hollow open celled sponge. D: 'Sponge by vacuum infusion' variations. E: Larger size 'Sponge by vacuum infusion' variations. Vx-20/13 and Vx-20/14 did not keep the dimensions of the original sugar cube. V-20/20 is the middle third part cut out of from a larger sponge ($5\,\mathrm{cm} \times 15\,\mathrm{cm} \times 3.5\,\mathrm{cm}$). F: Side of V-20/20 on the cutting plane. V-20/20 has a different structure in the center (area within highlight). G: 'Sponge by foaming' variations. F-1/5 had the least foaming agent and became the most dense one. H: Foaming the curing silicone produced 'inhomogeneous' sponges. On the left an example of how a specimen was cut out of the fabricated sponge. A sponge cured in the oven produced a bulge on top of the sponge as if it was a bread (second from the left). The two sponges on the right were cured in a microwave. These do not have a bulge on the top but have a few large air pockets. I1: Contact stress distribution characteristic of M-20/16 on a flat surface. The lighter (yellow) areas on the edges experience a higher contact pressure than the middle red area. Also some black spots (no contact stress) are seen. I2: These black spots seem to coincide with holes in the surface of the sponge. I3: A piece of the sponge was cut out to reveal a denser cell structure near the walls, see highlight. The surface shown in I2 is the bottom side in this figure.

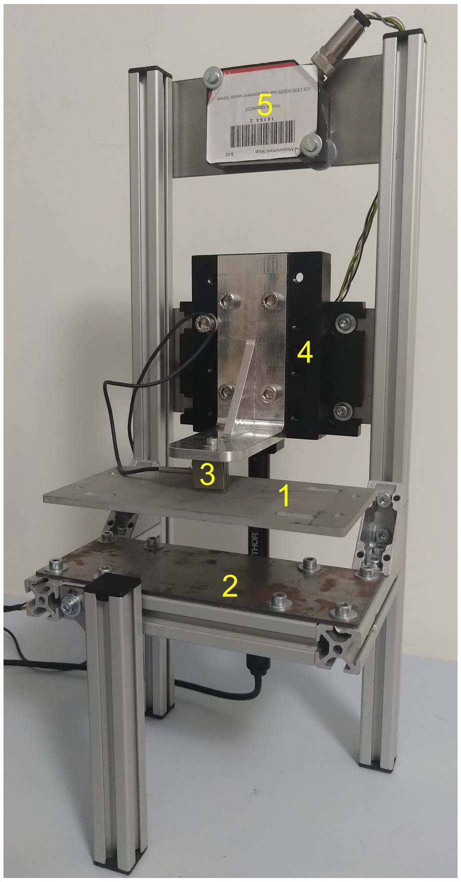

Fig. 21: Setup used to compress backings and measure the compression stress-strain characteristic. A backing material is placed in between rigid plates (1) and (2). Plate (1) is connected via a force sensor (3) to a linear actuator (4). A fixed laser distance sensor (5) measures distance to the actuator.

			Compression moduli [kPa] (Compression stress [kPa] /Compression strain [m/m])						
		mean	std	mean	std	mean	mean	mean	mean
At compression strain [%] -->		17		40		7	7.4	12.3	31.1
Backing variation (names below)									
H-2		2.5		6.5					
H-3		5.3		12.1					
H-4		7.3		15.8					
S-20/10		3.9		10.0					
S-20/12		11.1		21.6					
S-4/20		11.7		20.6					
S-20/14						17.9			25.3
S-20/16						48.8		64.0	
S-20/20						104.5	106.2		
I-O1		2.5		1.2					
I-O2		3.2		1.5					
I-O3		3.9		1.8					
I-C1		8.4							
I-C2		10.3							
I-C3		12.4							
M-20/13		3.6		4.0					
M-20/14		4.7		5.1					
M-20/15		6.1		6.2					
M-20/16		9.4		8.9					
V-20/13		0.6		1.3					
V-20/14		1.5		2.1					
V-20/15		2.2		3.2					
V-20/16		3.7		4.8					
V-20/20		4.8		8.4					
F-1/2-3		1.0		1.2					
F-1/2-2		2.3		1.9					
F-1/3.5		2.6		2.4					
F-1/2-1		2.7		2.4					
F-1/5		17.4		19.4					
P-S forward		5.6	0.1	3.5	0.1				
P-S return		2.6	0.0	1.9	0.0				
P-M forward		8.0	0.1	4.3	0.0				
P-M return		4.7	0.1	2.7	0.0				
P-H forward		10.5	0.1	5.6	0.0				
P-H return		4.8	0.1	3.1	0.0				

Fig. 22: Compression moduli of the backing variations. The closed Inflatable variations (IC-x) and the Silicone variations S-20/14 to S-20/20 are not measured at 40% strain, since they were too stiff or would fracture. 'Forward' refers to the compression stroke. Only the PUR-sponges (P-x) are measured on the return (relaxation) stroke.

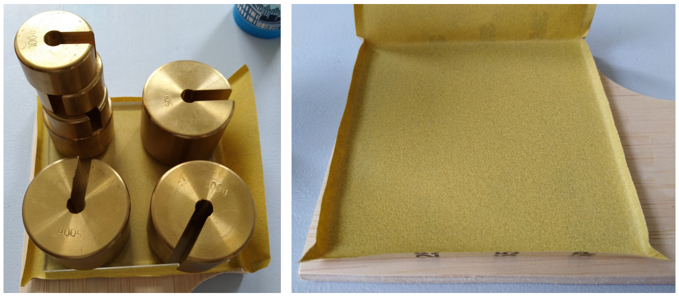

Fig. 23: Fabrication of a preload sensitive film. Left: Sandpaper is glued (wood glue) onto a wooden multiplex board. Weights are applied on top of a flat PMMA sheet to press the sandpaper on the wood while it dries. Right: The edges are folded inwards to create a mould in which a 1 mm layer of silicone is cast.

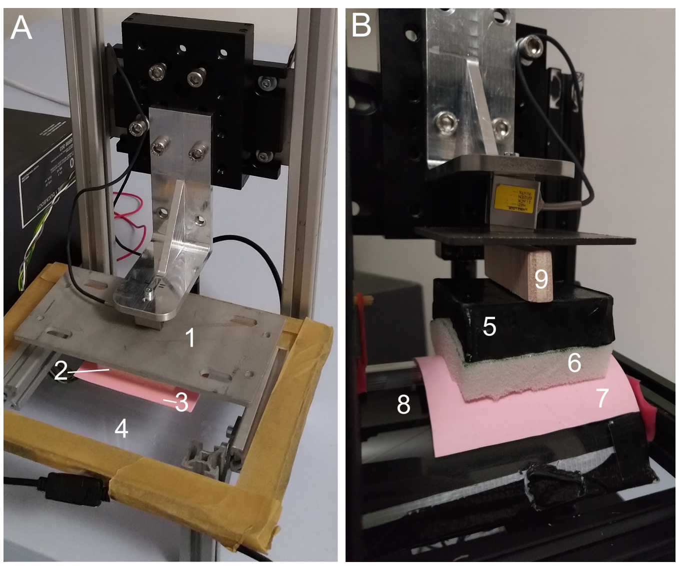

Fig. 24: Setups used to measure the conversion of light intensity captured from the preload sensitive film to contact stress. A: Setup used for the conversion measurement on the flat substrate. The preload sensitive film (3) has a PUR-sponge cuboid (2) on its top side to account for misalignment and surface irregularities. The film lies on the flat substrate into which a LED strip shines (4). The LED strip is attached with brown type. A flat panel (1), at the end of a force sensor and linear actuator, presses onto the sponge. A camera was placed onto the table (blue) and made a picture of the rough surface of the film. B: Setup used for the conversion measurement on the curved substrate. The film (7) has the same sponge (6) on top. On top of the sponge sits the rigid backing 'R-C' (5). A linear actuator presses R-C onto the sponge, via a wooden beam (9). The curved substrate (8) is illuminated with a LED strip, for FTIR, and attached with black tape. The camera is placed below the glass (in the same way as in the experiment sec.3.1.3).

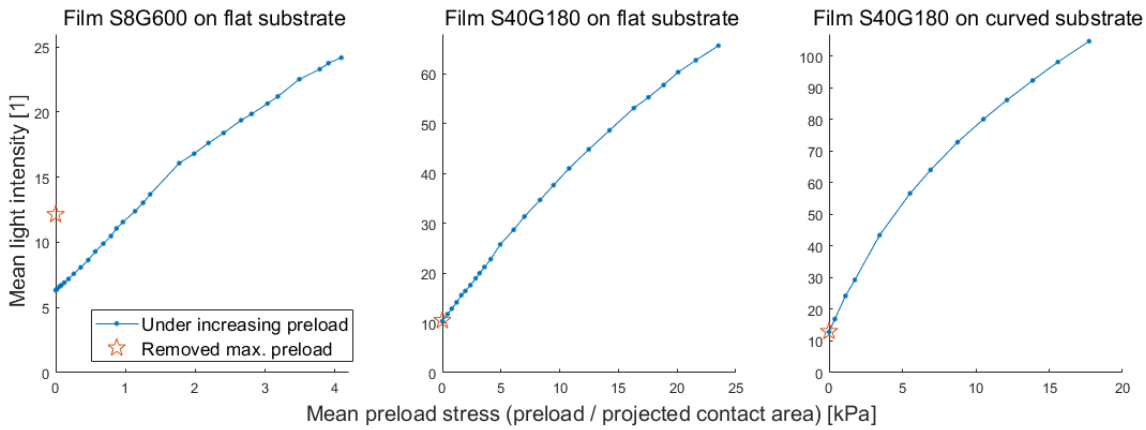

Fig. 25: Conversion relation between the mean light intensity measured with the conversion setups (fig.24) and the mean preload stress. Shutter time of the camera was 1/60 s for S40G180 on the curved substrate, and was 1/500 s for the other cases, giving S40180 a higher mean light intensity on the flat substrate than S8G600. The softer film S8G600 sticks a bit to the substrate giving a higher mean light intensity at no preload right after removing the maximum load, compared to the start of the preload, indicated by the star.

Appendix B
Experiment extras

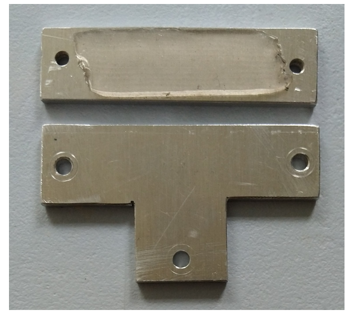

Fig. 26: Clamp used to fix the tail of an adhesive system to the linear actuator. The clamp consists of two plates which connect with 2 bolts on the sides. Double sided tape (GrippTek) was placed on one of the plates to increase the friction force holding the tail in place. The other plate has an extra hole through which it is connected with a bolt to the linear actuator’s moving stage.

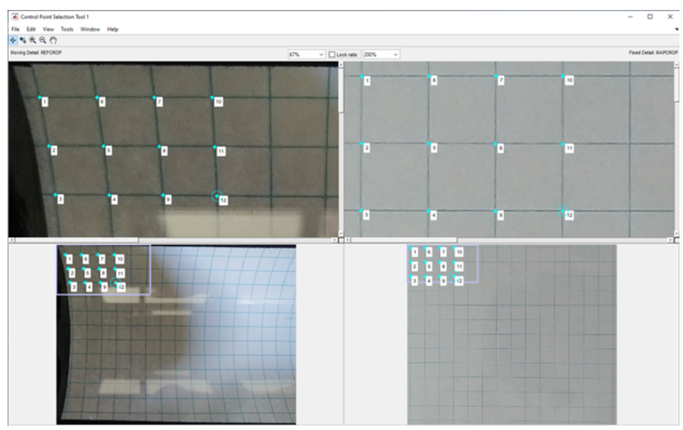

Fig. 27: View of the function ’cpselect’ in Matlab. The function lets the user choose which points coincide with a reference image and the distorted image. The image on the bottom left is a paper with 5 mm by 5 mm grid placed on the curved glass substrate. On the bottom right is the same paper on a flat surface. The top figures are close ups used to select the coinciding points. 100 control points were chosen at intersecting lines. With the control points a mapping is made with the function ’fitgeotrans’ in Matlab. This mapping can be seen in figure 28A-D.

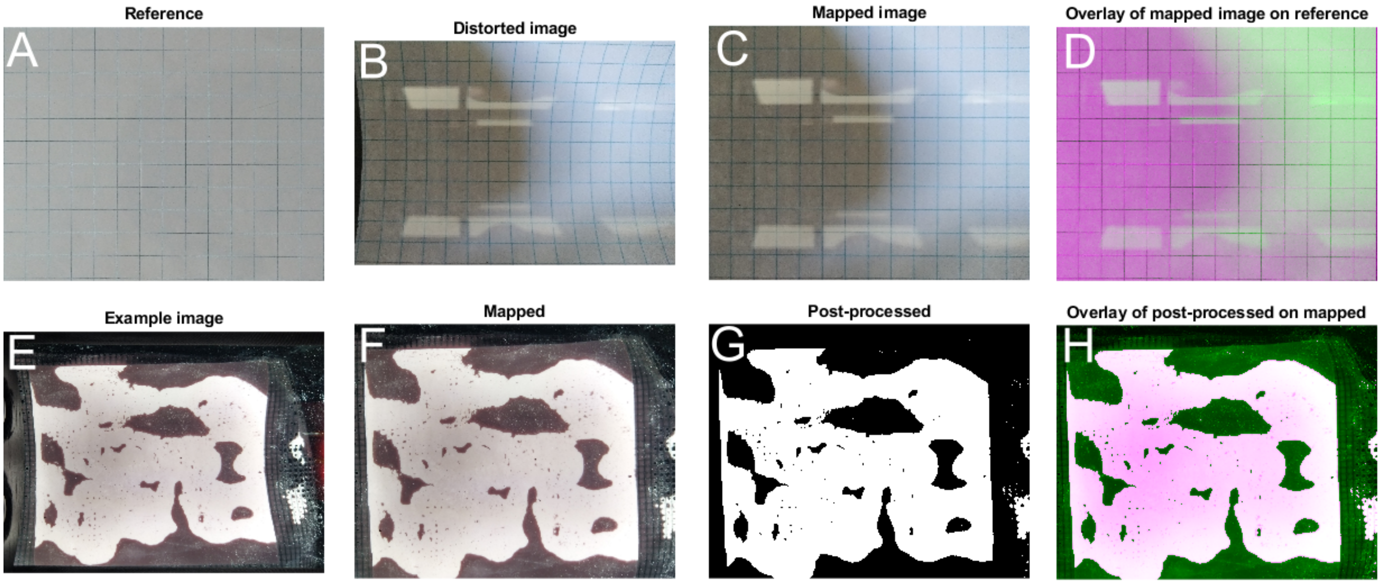

Fig. 28: Image post processing to account for distortion and to filter the contact area. With the reference image of a flat plane (A) and the distorted image of curved substrate's surface area (B), a map function is made with the Matlab function 'fitgeotrans'. With this function the distorted image of the curved substrate's surface area can be mapped to an image in which the contact area per pixel is even throughout the image (C). As a check the reference image is laid over the mapped image (D). An adhesive system making contact with the substrate (E) is mapped with the map function (F). Later this image is filtered, and a brightness threshold is used to decide which parts are in contact (brighter areas)(G). As a check the post-processed image is laid over the mapped image. Areas that are lighter in the mapped image than in the post-processed image are greenish, and areas that are darker in the mapped image are pinkish (H).

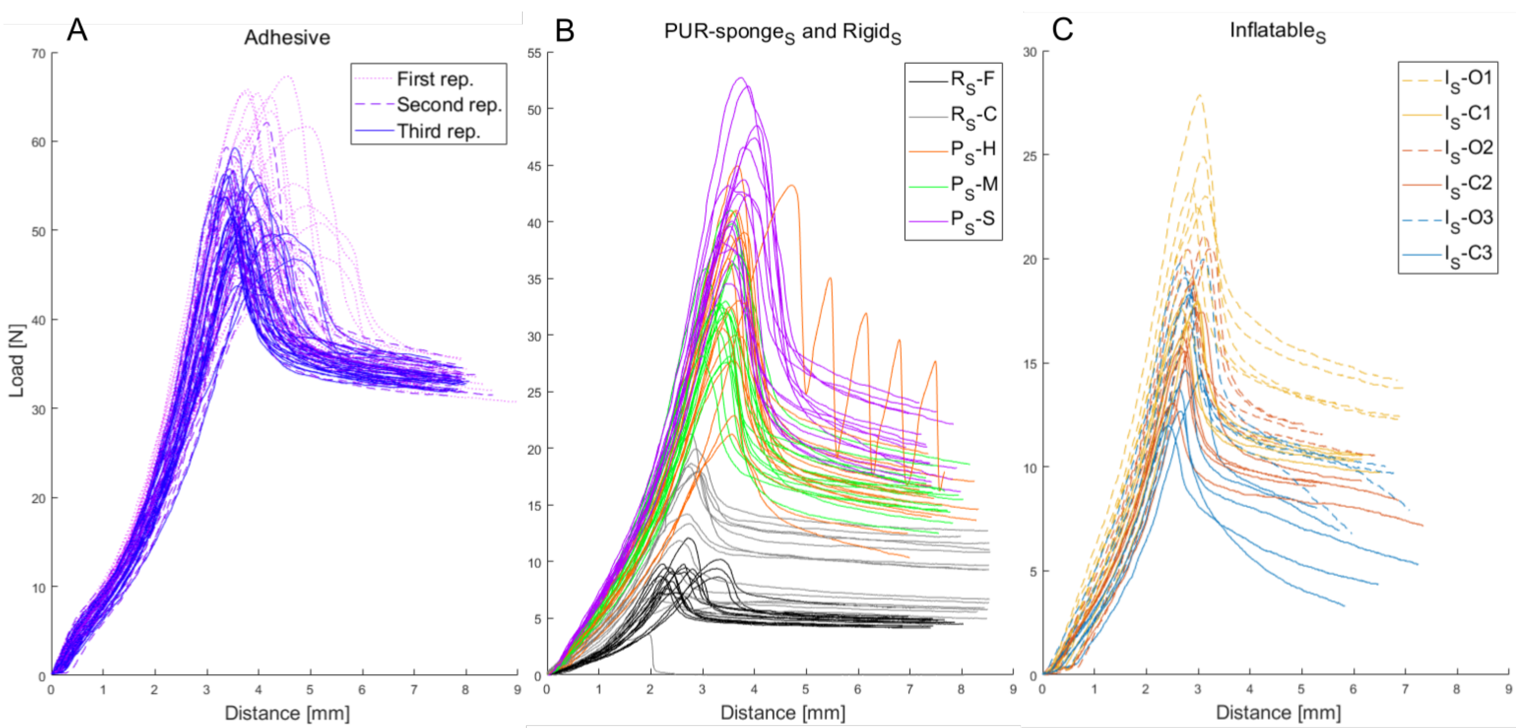

Fig. 29: Load capacity versus distance relations. A: Adhesive specimens tested for three repetitions. B: PUR-sponge and Rigid systems. Each variation had 5 specimens which were tested for 3 repetitions C: Inflatable system. Each variation was tested for 5 repetitions.

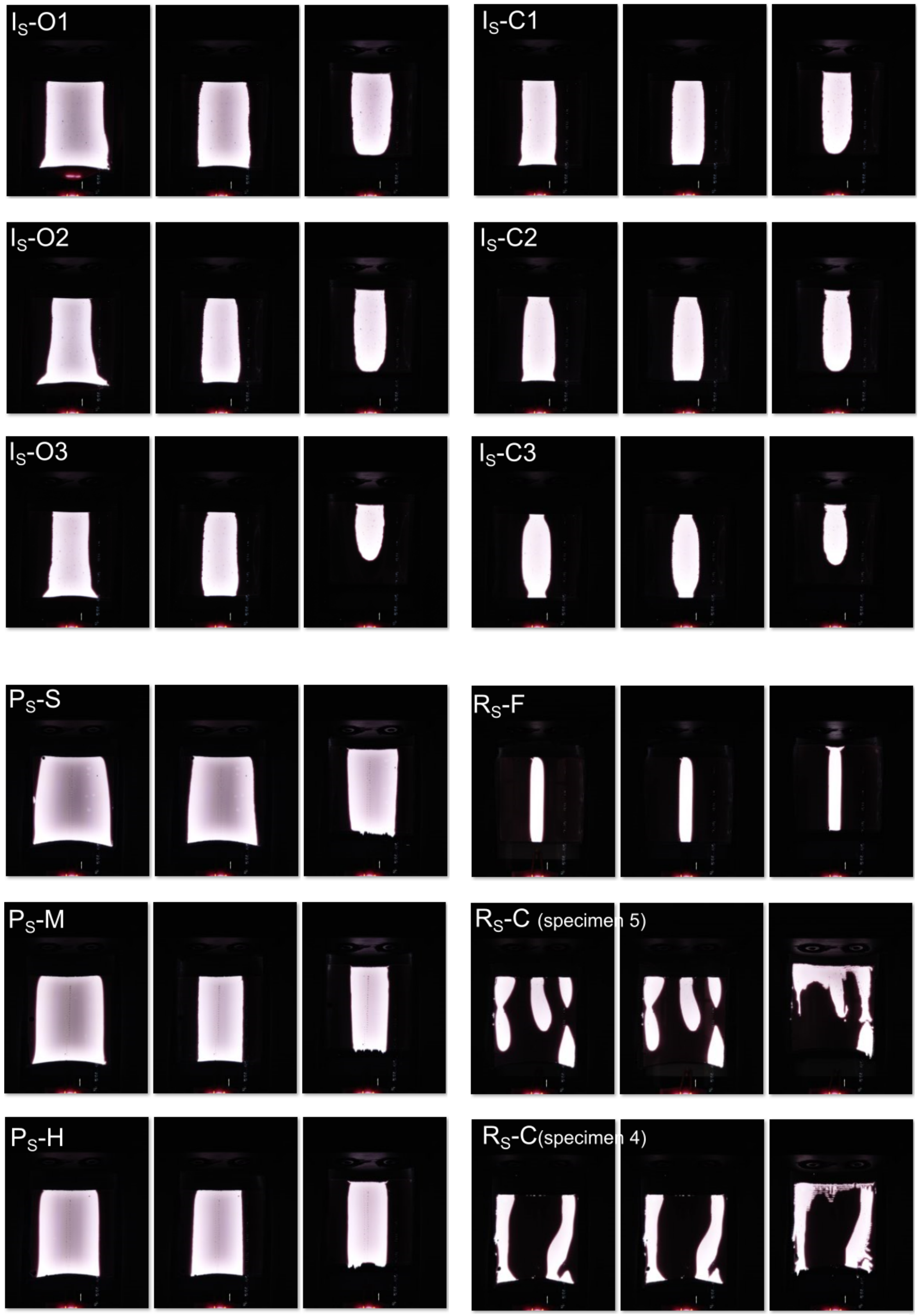

Fig. 30: Example contact areas of the adhesive systems. Of each system type variation, one specimen is shown in the three test phases. From left to right (per system type variation, e.g. $\mathrm{I_S} - O1$, photo group): end of preload phase, end of rest phase, end of load phase (due to sliding of the adhesive system these are higher up in the photo). For $\mathrm{R_S}$-C there are two specimens shown since their contact area shape characteristic differed. The contact characteristic of specimen 5 belongs to the specimens with a higher load capacity than the ones with a contact area similar to specimen 4.

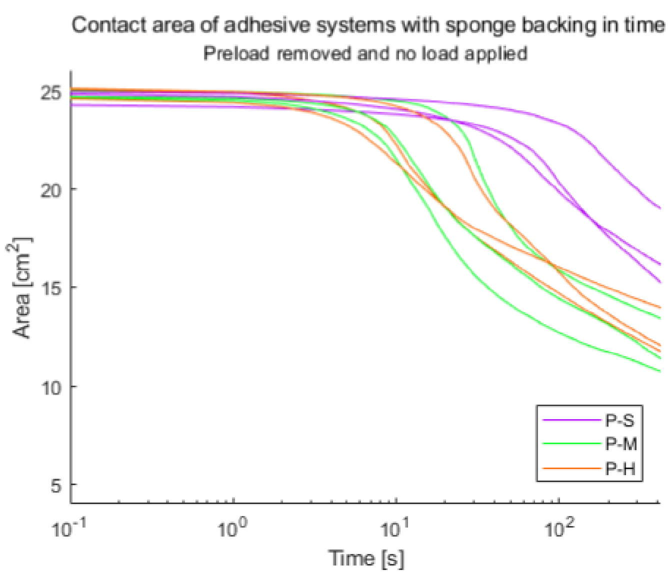

Fig. 31: Contact area in time for the PUR-sponge system. The system was preloaded until full contact was made with the curved substrate. No load was applied, but still, contact area decreased in time. Contact area decreases more slowly for P-S than P-M and P-H.

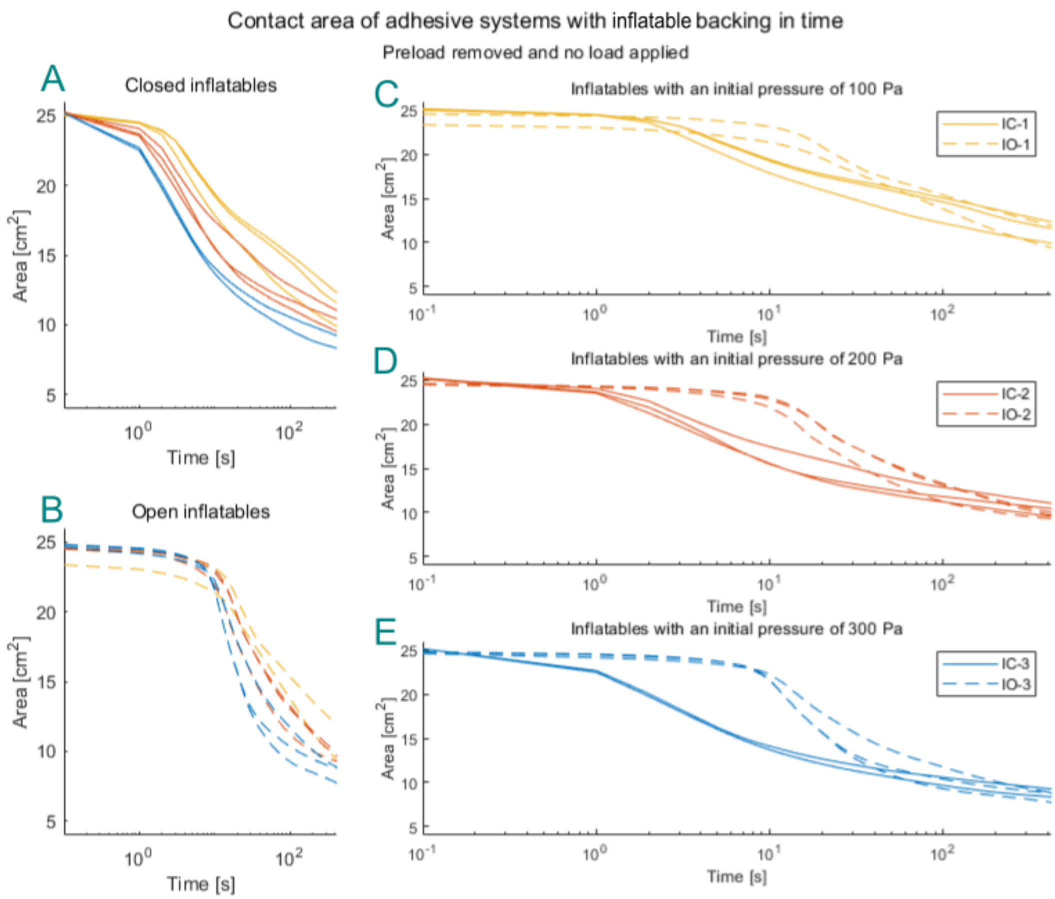

Fig. 32: Contact area in time for the Inflatable system. The system was preloaded until full contact was made with the curved substrate. No load was applied, but still, contact area decreased in time. A: Contact area decreases more slowly for closed variations with a lower internal pressure. B: Contact area decreases more slowly for open variations with a lower internal pressure. C-E: Contact area decreases more slowly for an open Inflatable than an closed Inflatable with the same initial pressure.